Vol. 651: 23–43, 2020
https://doi.org/10.3354/meps13476

MARINE ECOLOGY PROGRESS SERIES
Mar Ecol Prog Ser

Published October 1

Ice algae resource utilization by benthic macro- and megafaunal communities on the Pacific Arctic shelf determined through lipid biomarker analysis

Chelsea Wegner Koch[1,*], Lee W. Cooper[1], Jacqueline M. Grebmeier[1], Karen Frey[2], Thomas A. Brown[3]

[1]Chesapeake Biological Laboratory, University of Maryland Center for Environmental Science, Solomons, MD 20688, USA
[2]Graduate School of Geography, Clark University, Worcester, MA 01610, USA
[3]Scottish Association for Marine Science, Oban PA37 1QA, UK

ABSTRACT: We studied ice algae utilization by benthic fauna from the northern Bering and Chukchi Seas using highly branched isoprenoid (HBI) biomarkers. We assessed whether various food acquisition strategies influence the observed HBI signatures. The proportion of phytoplankton to ice algae-sourced HBIs was determined through the H-Print approach that is presumed to reflect the percentage of sea ice organic carbon (iPOC) incorporated into tissues, relative to phytoplankton organic carbon. Cluster analysis separated 3 groups based on location and feeding strategy that were significantly influenced by annual sea ice persistence. Ice algae utilization was most significant in the northeast Chukchi Sea, where seasonal sea ice was present the longest. General feeding strategy was determined to be a significant factor in the degree of ice algae utilization. Predominant deposit feeders (both surface and subsurface) used more ice algae relative to suspension feeders. Organic carbon incorporated by predominant suspension feeders was primarily phytoplankton-based. The vast majority of all organisms sampled (~90%) incorporated a measurable quantity of iPOC. Sipunculids and brittle stars had the highest relative dependence on ice algae, while other taxa displayed plastic dietary responses, including the suspension/surface deposit feeder *Macoma calcarea*. This study indicates that ice algae are widely utilized in Pacific Arctic benthic food webs, but most benthic organisms displayed flexibility in consuming the available food sources. The elevated utilization of ice algae by deposit feeders may prove to be a disadvantage for these organisms if they cannot adapt to the ongoing decline of iPOC as seasonal sea ice declines.

KEY WORDS: Highly branched isoprenoid · Biomarker · Sea ice · Benthic invertebrates · Ice algae · Phytoplankton · Arctic benthos · Organic carbon

1. INTRODUCTION

Microalgal primary production on the Pacific Arctic continental shelves is partitioned between ice-associated (sympagic) and pelagic diatoms, and depends on seasonal ice cover dynamics, nutrient availability, and water column stratification (Hill et al. 2018, Selz et al. 2018). Strong sympagic–pelagic–benthic coupling has sustained rich benthic ecosystems on this shallow shelf system (Iken et al. 2010, Dunton et al. 2014, Grebmeier et al. 2015). However, declining sea ice cover and persistence along with changes in the timing of the sea ice cycle are likely to disrupt this ecosystem structure (Grebmeier et al. 2006a, Leu et al. 2011, Kędra et al. 2015, Moore et al. 2018). Sea ice has declined overall in the Arctic, with pronounced losses in the Bering and Chukchi Seas (Serreze & Meier 2019). The winter of 2017–2018 marked the record

*Corresponding author: cwegner@umces.edu

low maximum sea ice extent for the northern Bering Sea, reaching only 46% (411 500 km^2) of the 1979–2016 mean maximum extent (Thoman et al. 2020). These were levels that were not previously predicted to occur until the 2030s (Stabeno & Bell 2019).

With the increasing open-water season for the Pacific Arctic, there are a number of possible outcomes that will impact trophic stability and function as a result of changes in the timing, quality, and quantity of the basal food source (Moore & Stabeno 2015). Lower trophic level consumers coordinate life cycles (i.e. spawning, growth, foraging) with the early spring bloom containing sympagic microalgae, where a mismatch in timing could be detrimental to the food web (Søreide et al. 2010, Leu et al. 2011). Ice algae are a high-value food source because of their high polyunsaturated fatty acid composition (Falk-Petersen et al. 1998, McMahon et al. 2006, Søreide et al. 2010, Wang et al. 2014) and high sinking rates (Legendre et al. 1992, Riedel et al. 2006) relative to phytoplankton. Although overall primary production is predicted to increase in the Arctic with global warming (Arrigo & van Dijken 2015, Lewis et al. 2020), it would likely coincide with an increasing proportion of small pelagic algae with a lower sinking potential (Li et al. 2009) and a decrease in sympagic productivity.

As a result of these changes in primary production, the organic carbon flow in the Pacific Arctic is hypothesized to increase through pelagic trophic chains to the detriment of the benthic ones, which will have a large impact on the whole food web in terms of both quality and standing stock (Kędra et al. 2015, Moore & Stabeno 2015). The shift to a pelagic-dominated food web, together with access to ice-free waters, is likely to lead to population increases in foraging pelagic fish, along with water column feeding whales and seabirds (Moore & Huntington 2008, Kędra et al. 2015). As a result, there are expected to be reductions and redistributions of benthic populations that serve as the prey base for higher trophic predators including walruses, bearded seals, spectacled eiders, and gray whales (Grebmeier et al. 2006b, Moore & Huntington 2008, Jay et al. 2014, Moore & Stabeno 2015). A shift has already been observed in the northern Bering Sea benthic communities, with northward contractions in dominant species and declines in benthic biomass (Overland & Stabeno 2004, Grebmeier et al. 2006b, 2018). Therefore, monitoring changes in the functioning of the benthos is critical for identifying a larger ecosystem shift.

Various approaches have been used to assess the benthic response to sea ice retreat and food availability on Arctic shelves. Given that sea ice algae account for only 4–26% of overall production on Arctic shelves (Legendre et al. 1992, Arrigo 2014), uncertainties remain about the significance of this food source and its potential decline. However, these values may be an underestimate on the Chukchi shelf, where ice algae significantly exceed phytoplankton biomass and productivity in the spring (Gradinger 2009). Despite the uncertainty in the actual proportion of sea ice algae that support the benthic-based food web, the pulsed timing and high quality of the largely ungrazed food source is thought to increase its trophic significance (Søreide et al. 2010, Leu et al. 2011, 2015, Dezutter et al. 2019). It has been an ongoing imperative to distinguish the sympagic and pelagic organic matter sources and trace their flow to the benthic and Arctic food webs.

The compositions of ice algae and phytoplankton communities are complex and have been difficult to unequivocally distinguish, since numerous taxa share both environments. Stable isotopes have allowed the detection of an enriched carbon signature in ice algae, yet these values can vary in space and time with the bloom progression and include additional potential sources (e.g. terrestrial, bacterial, etc.) which makes them unreliable indicators alone (Tremblay et al. 2006, Gradinger 2009). Essential fatty acids are another tool that have advanced our ability to trace organic carbon sources in the Arctic but still lack unambiguous source specificity between the ice and open-water regimes (McMahon et al. 2006, Budge et al. 2008, Schollmeier et al. 2018). The use of fatty acids assumes that sea ice organic matter is comprised primarily of diatoms and can best be represented by a fatty acid marker common to diatoms (Budge et al. 2008, Wang et al. 2014). However, the community composition of pelagic blooms is complex and is further compounded by the transition from diatoms to dinoflagellates as blooms progress seasonally in the Pacific Arctic (Szymanski & Gradinger 2016, Hill et al. 2018, Selz et al. 2018). Compound-specific stable isotope analyses of these fatty acids have further refined the distinction between organic carbon sources but still remain equivocal (McMahon et al. 2006, Budge et al. 2008, North et al. 2014, Wang et al. 2014, Kohlbach et al. 2016, 2018, Mohan et al. 2016, Schollmeier et al. 2018).

Highly branched isoprenoid (HBI) lipids provide an advantage over these other methods to distinguish sympagic and pelagic resources in Arctic food webs. C_{25} HBI lipids are produced by a small number of commonly occurring diatoms and serve as biomarkers based upon the number and position of double

bonds (Volkman et al. 1994, Belt et al. 2007). A monounsaturated C_{25} HBI, termed 'Ice Proxy' with 25 carbon atoms (IP_{25}), is synthesized by 3 or 4 sympagic diatom species in the Arctic (Belt et al. 2007, Belt & Müller 2013, Brown et al. 2014b, Limoges et al. 2018). Owing to the stability of this compound and its persistence in the environment, IP_{25} is a reliable proxy for paleo sea ice reconstructions (Stein et al. 2016, Belt 2018). Di- and tri-unsaturated structural isomers provide further context for these interpretations. These isomers include a diene (HBI II), associated with sea ice in both polar regions, and a triene (HBI III), found globally in open waters and marginal ice zones (see review by Belt 2018). HBI III has also proven to be a reliable pelagic biomarker when used in a sea ice index validated by numerous well-resolved paleo sea ice reconstructions (Müller & Stein 2014, Stein et al. 2017, Kremer et al. 2018). However, modern ecological applications of these HBIs are gaining interest. IP_{25} is chemically stable once grazed and assimilated by consumers, enabling us to track the trophic transfer of sea ice carbon (Brown & Belt 2012). Measuring the relative proportion of sympagic (IP_{25} and HBI II) to pelagic HBIs (III) creates an index termed H-Print, which provides further insight into resource utilization in Arctic food webs (Brown et al. 2014c).

As with previously described methods, there are limitations to consider with H-Print and the use of HBIs more broadly. In some circumstances, HBI III may be more susceptible to abiotic degradation in the water column based on the extent of algal senescence and the comparative sinking rates of sea ice and open water diatoms, with sea ice diatoms more rapidly removed from the photic zone (Rontani et al. 2019). There is also evidence that HBI III can at times be co-synthesized within or under sea ice (Amiraux et al. 2019). However, this has been attributed to entrapment of pelagic diatoms, as the identified sources of HBI III (from the genus *Rhizosolenia*) are not ice-associated and may have been a site-specific phenomenon with minimal impacts on HBI indices. Additionally, the specific assimilation and depuration rates of HBIs in primary consumers are largely unknown. Other studies concluded that HBIs do not bioaccumulate in higher trophic organisms and represent seasonal observations (Brown et al. 2014a, 2017, 2018). However, the advantages of HBIs over previously described methods include the ability to more definitively distinguish sea ice and pelagic carbon sources.

The application of HBI measurements to the Pacific Arctic food web could provide promising new insights into the significance of ice algae in this productive continental shelf system. With this objective in mind, we applied the H-Print method to track ice algae utilization by benthic consumers of the northern Bering and Chukchi Seas to determine which organisms and/or feeding strategies are more reliant on sympagic carbon. Based on observed shifts in benthic biomass and dominant species, along with the phenology and quality of algal blooms in the northern Bering Sea over the last decade (Grebmeier et al. 2018), we hypothesized that there are differences in ice algae utilization among feeding strategies and taxa. To test this hypothesis, a range of benthic invertebrates (epifaunal and infaunal) were collected over the summer of 2018 and analyzed for their HBI content with respect to location, feeding strategy, and overlying sea ice conditions. Determining the partitioning of sea ice and pelagic organic carbon resources may identify the organisms that are more vulnerable to a changing food supply as a result of declining sea ice and their ability to adapt to these changes.

Owing to a lack of data on HBI retention and depuration rates in invertebrates, we also conducted a natural depuration experiment using bivalves to determine the turnover rates of HBIs relative to the time of consuming the organic matter. Establishing a baseline of HBI depuration rates is necessary to accurately estimate the time period of foraging reflected in the H-Print values. Since HBI III is not specific to polar regions, it was practical to measure depuration rates of this HBI from temperate clams. This experimental design allowed us to fully remove natural introduction and prevent recirculation of HBI III using a flow-through filtration system. We used *in situ* temperate conditions in Chesapeake Bay, USA, because it was not feasible to maintain the flow-through system at sustained Arctic temperatures; therefore, this experiment serves as a starting point for addressing these questions. We acknowledge that HBI III and IP_{25} may behave differently, but nevertheless this experiment can serve as a general baseline to measure HBI retention in macrofaunal tissue.

2. MATERIALS AND METHODS

2.1. Study site

Sampling stations were located in regions of high benthic biomass influenced by Pacific water inflow across the shallow (<100 m) continental shelf of the northern Bering and Chukchi Seas (Fig. 1). These regions are annually sampled as part of the Distrib-

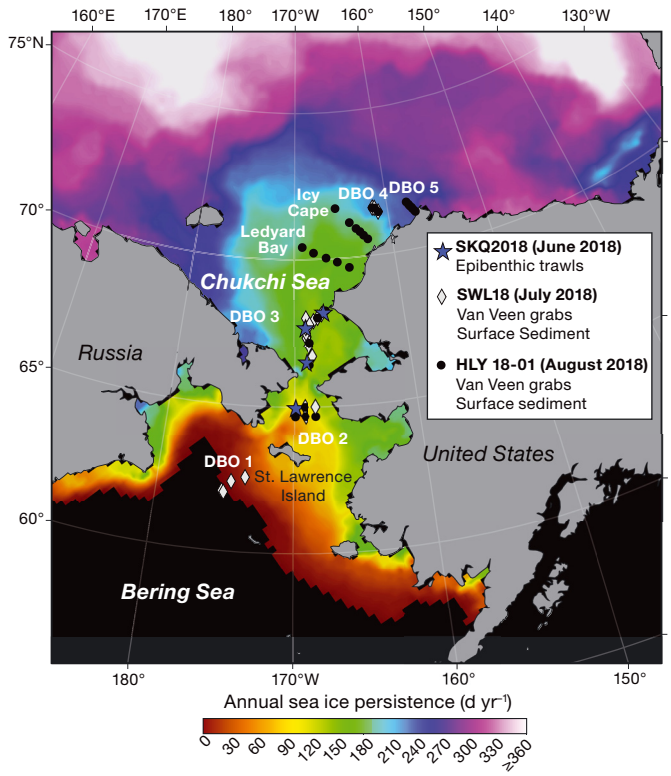

Fig. 1. Sampling locations in the northern Bering and Chukchi Seas in June (ASGARD, SKQ2018, blue stars), July (Distributed Biological Observatory [DBO], SWL18, black dots), and August (DBO, HLY18-01, gray diamonds) 2018 with corresponding sampling methods. Sea ice persistence is shown as days of sea ice cover (i.e. >15% concentration) per year, which was defined as the sea ice period from 14 September 2017 through 15 September 2018. The areas in black were ice-free throughout the entire year-long period

uted Biological Observatory (DBO), which serves as a change detection array and was formally established in 2010 with time series observations spanning over 30 yr (Grebmeier et al. 2010, Moore & Grebmeier 2018). Our sampling spanned 5 DBO regions (DBO 1–5) (https://dbo.cbl.umces.edu) and 2 additional transects. DBO 1 is located near the winter-only polynya that forms south of St. Lawrence Island in the northern Bering Sea; DBO 2 is in the Chirikov Basin south of Bering Strait; DBO 3 is in the southeast Chukchi Sea, where organic-rich material settles out north of Bering Strait; DBO 4 is in the northeast Chukchi Sea on the southeastern flanks of Hanna Shoal; and DBO 5 is a transect across Barrow Canyon (Grebmeier et al. 2015). The Icy Cape (IC) transect has high benthic biomass due to sustained advection of organic carbon from more productive regions (Feder et al. 1994). The Ledyard Bay (LB) transect is in the Chukchi Sea and was only sampled for surface sediments.

2.2. Sea ice persistence

Sea ice persistence data were determined from sea ice concentrations obtained from the Special Sensor Microwave Imager/Sounder (SSMIS) on the Defense Meteorological Satellite Program satellites, and compiled by the National Snow and Ice Data Center (www.nsidc.org). A 15% ice concentration threshold was set to identify days of sea ice presence in the Pacific Arctic region (Frey et al. 2015). We then summed the number of days with sea ice present (>15%) per pixel, from 14 September 2017 through 15 September 2018. Discrete sea ice persistence values were obtained for each of the sampling locations by extracting the value of the pixel at each location (Fig. 1). The use of annual persistence, rather than confined to the sampling period, allowed for the inclusion of winter sea ice conditions that would contribute to the lack of or delay in a spring bloom and account for the deposition of organic matter available in the sediments prior to sampling.

2.3. Benthic sampling

Organisms were collected on board the CCGS 'Sir Wilfrid Laurier' (SWL18; 16–23 July 2018) and the USCGC 'Healy' (HLY18-01; 7–24 August 2018) as part of the DBO program (Table 1, Fig. 1). Additional samples were collected opportunistically on board the RV 'Sikuliaq' (SKQ2018; 4–25 June 2018) as part of the Arctic Shelf Growth, Advection, Respiration and Deposition (ASGARD) Rate Measurements Project of the Arctic Integrated Ecosystem Research Program, which overlapped with the DBO 2 and 3 regions (Table 1, Fig. 1).

Epibenthic megafauna were collected from trawl surveys on SKQ2018 using a modified plumb-staff beam trawl (2.26 m opening; 7 mm mesh net; 4 mm cod end liner). Trawl sample biomass was dominated by echinoderms, mollusks, crustaceans, sponges, ascidians, and bryozoans. Organisms were either sorted from the full catch or from a well-defined, well-mixed subsample. All samples were sorted by species, genus, or distinct morphotype depending on the level of identification possible on board. Surface sediments were not collected on this cruise.

Benthic macrofauna (>1 mm, including megafauna) were collected on the SWL18 and HLY18-01 cruises using a 0.1 m^2 van Veen grab weighted with 32 kg lead. Grab sample biomass was dominated by bivalves, polychaetes, crustaceans, sipunculids, echinoderms, and anthozoans. The grab was gently lowered

Table 1. Station summary for the ASGARD cruise SKQ2018 and the Distributed Biological Observatory (DBO) cruises SWL18 and HLY18-01

Sampling date (yyyy-mm-dd)	Station ID	Latitude (°N)	Longitude (°W)	Sampling depth (m)	Cruise
2018-06-11	DBO 2.4	64.964	169.889	46	SKQ2018
2018-06-11	Diomede	65.753	168.871	30	SKQ2018
2018-06-14	DBO 3.8	67.670	168.951	51	SKQ2018
2018-06-15	DBO 3.3	68.189	167.308	49	SKQ2018
2018-06-12	CNL3	66.510	168.959	56	SKQ2018
2018-07-16	SLIP1	62.009	175.063	80	SWL18
2018-07-16	SLIP2	62.049	175.206	82	SWL18
2018-07-16	SLIP3	62.391	174.569	72	SWL18
2018-07-17	SLIP5	62.558	173.558	66	SWL18
2018-07-18	UTBS2	64.681	169.100	45	SWL18
2018-07-18	UTBS1	64.992	169.140	49	SWL18
2018-07-18	DBO 2.7	65.000	168.220	46	SWL18
2018-07-19	UTN1	66.709	168.398	35	SWL18
2018-07-19	UTN2	67.050	168.728	46	SWL18
2018-07-19	UTN3	67.331	168.905	50	SWL18
2018-07-20	UTN4	67.500	168.909	50	SWL18
2018-07-20	SEC4	68.013	167.866	54	SWL18
2018-07-21	SEC1	67.672	168.930	50	SWL18
2018-07-21	UTN6	67.740	168.441	51	SWL18
2018-07-21	SEC2	67.784	168.602	50	SWL18
2018-07-21	SEC3	67.899	168.236	59	SWL18
2018-07-21	UTN7	68.000	168.929	58	SWL18
2018-07-21	SEC5	68.128	167.493	51	SWL18
2018-07-22	DBO 4.4	71.588	161.401	49	SWL18
2018-07-22	DBO 4.5	71.610	161.615	44	SWL18
2018-07-23	DBO 4.3	71.454	161.036	49	SWL18
2018-08-08	UTBS2A	64.671	168.234	39	HLY18-01
2018-08-08	UTBS1	64.991	169.146	49	HLY18-01
2018-08-09	UTBS5	64.672	169.926	48	HLY18-01
2018-08-09	T2	67.164	168.664	47	HLY18-01
2018-08-10	SEC4/DBO 3.5	68.015	167.880	51	HLY18-01
2018-08-10	SEC5/DBO 3.4	68.136	167.492	48	HLY18-01
2018-08-11	SEC1/DBO 3.8	67.677	168.957	51	HLY18-01
2018-08-11	SEC2/DBO 3.7	68.246	167.126	51	HLY18-01
2018-08-12	IC-10	71.705	165.603	43	HLY18-01
2018-08-13	IC-6	71.195	164.202	45	HLY18-01
2018-08-13	IC-8	71.449	164.919	43	HLY18-01
2018-08-13	IC-9	71.601	165.304	43	HLY18-01
2018-08-14	IC-1	70.580	162.491	39	HLY18-01
2018-08-14	IC-2	70.717	162.857	43	HLY18-01
2018-08-14	IC-3	70.849	163.187	45	HLY18-01
2018-08-15	DBO 4.3	71.351	161.396	49	HLY18-01
2018-08-15	DBO 4.4	71.481	161.505	49	HLY18-01
2018-08-15	DBO 4.5	71.610	161.615	47	HLY18-01
2018-08-17	DBO 5.1	71.247	157.135	45	HLY18-01
2018-08-17	DBO 5.2	71.289	157.221	56	HLY18-01
2018-08-17	DBO 5.4	71.373	157.380	116	HLY18-01
2018-08-17	DBO 5.5	71.410	157.450	131	HLY18-01
2018-08-17	DBO 5.6	71.454	157.553	120	HLY18-01
2018-08-17	DBO 5.7	71.495	157.627	96	HLY18-01
2018-08-17	DBO 5.8	71.536	157.711	75	HLY18-01
2018-08-17	DBO 5.10	71.626	157.901	64	HLY18-01

onto the deck and a trap door on the top was opened prior to the full grab opening in order to sample relatively undisturbed surface sediments for HBI analysis. The sediments were collected by skimming the surface with a metal spatula. Prior studies have established from radiocesium activities that the surface sediments on the Bering and Chukchi shelf (<100 m) reflect recent deposition, and that due to bioturbation, surface sediments recovered from the tops of cores are as well-mixed as those from the tops of van Veen grabs (Cooper et al. 1998, Cooper & Grebmeier 2018). Organisms were sieved through 1 mm mesh sieve screens, live sorted, and identified to the lowest taxonomic level practical on board. Organisms from all 3 cruises and sediments were placed in individual Whirl-pak® bags, immediately frozen (–20°C), and stored until analysis. All benthic fauna collected were classified by feeding strategy using the following 5 categories: suspension feeder (SUS), surface deposit feeder (SDF), subsurface deposit feeder (SSDF), suspension–surface deposit feeder (SUS/SDF), or predator/scavenger (P/S) based on previous studies (Table 2).

2.4. Biomarker extraction

All samples were freeze dried in the laboratory for 48 h, soft tissues were removed from shells as required, and samples were then homogenized by mortar and pestle. Approximately 1 g of dried sediment or 0.1–0.5 g of dried tissue were subsampled for analysis. Owing to the variable sizes and number of organisms per station, where there was often only 1 individual per taxon per grab, major taxa with more than 1 individual were grouped for analysis. This was intended to capture a representative HBI composition per species and/or feeding strategy at a particular station. HBI biomarkers were extracted from 78 surface sediment samples and 193 tissue samples. HBIs were extracted following established methods (Belt et al. 2012, Brown et al. 2014c). Briefly, an internal standard (10 µl) of 9-octylheptadec-8-ene (9-OHD, 1 µg ml^{-1}) was added to the sample before extraction to facilitate yield quantification. Samples were saponified in a methanolic KOH solution and

Table 2. Summary of taxa collected in 2018 for highly branched isoprenoid (HBI) biomarkers with assigned feeding strategy, cruise (SKQ: SKQ2018; SWL: SWL18; HLY: HLY18-01; see Table 1) and collection method, along with the Distributed Biological Observatory (DBO) sample regions (see Fig. 1; IC: Icy Cape). Feeding strategies were classified as SUS: suspension feeder; SUS/SDF: suspension/surface deposit feeder; SDF: surface deposit feeder; SSDF: subsurface deposit feeder; P/S: predator/scavenger. Sample size indicates number of stations with the species analyzed

Species	Sample size (n)	Feeding strategy	SKQ (trawls)	SWL (grabs)	HLY (grabs)	DBO sample regions
Holothuroidea						
Amphideima sp.	1	SUS[a]	X			2
Chiridota sp.	1	SDF[a]	X			2
Ocnus glacialis	2	SUS[b]	X			3
Myriotrochus sp.	1	SUS[a]		X		3
Ascidacea (Tunicata)						
Styela rustica	4	SUS[b]	X	X	X	2, 3, 5
Pelonaia corrugata	2	SUS[b]	X			2, 3
Boltenia ovifera	2	SUS[b]	X			2
Boltenia echinata	3	SUS[b]	X			3
Chelyosoma macleayanum	3	SUS[b]	X			3
Gastropoda						
Neptunea heros	3	P/S[b]	X			2
Neptunea communis	1	P/S[b]	X			2
Buccinum scalariforme	2	P/S[b]	X			2
Buccinum polare	2	P/S[b]	X			3
Cryptonatica affinis	5	P/S[b]	X			2, 3
Bivalvia						
Serripes lamperosii	7	SUS [a,b]	X	X	X	3
Macoma calcarea	37	SUS/SDF[c]	X	X	X	ALL
Ennucula tenuis	18	SSDF[c]		X	X	ALL
Nuculana pernula	2	SSDF[b]		X		3, 4
Astarte borealis	4	SUS[c]		X	X	IC, 4, 5
Yoldia hyperborea	11	SSDF[c]		X	X	3, IC, 4, 5
Mya truncata	2	SUS[b]		X		3
Mya sp.	1	SUS[b]		X		3
Musculus sp.	2	SUS[b]		X	X	IC, 4
Hiatella arctica	1	SUS[b]	X			3
Pandora sp.	1	SUS[b]			X	IC
Lysianassidae unidentified sp.	1	P/S[b]			X	IC
Nutricola sp.	2	SUS[b]			X	IC, 5
Polychatea						
Gattyana ciliata	1	SSDF[b]	X			2
Gattyana sp.	1	SSDF[b]	X			3
Eunoe sp.	1	P/S[b]	X			3
Nephtys sp.	8	P/S[b]		X	X	2, 3, 5
Pectinaria hyperborea	12	SSDF[b]		X	X	1, 3, 4, IC, 5
Maldane sp.	18	SSDF[b,c]		X	X	ALL
Echiurus echiurus	3	SDF[a]	X			3
Lumbrineris sp.	1	SSDF[b]				IC
Sipuncula						
Golfingia margaritacea	6	SDF[d]			X	3, IC, 5
Ophiuroidea						
Ophiura sarsii	3	SDF[b]		X		1, 4
Gorgonocephalus sp.	1	P/S[b]			X	5
Malacastroca (Decapoda)						
Pandalus eous	1	P/S[b]		X		1
Pagurus trigonocheirus	1	P/S[b]	X			2
Chionoecetes opilio	2	P/S[e]		X		1, 3
Malacastroca (Amphipoda)						
Isaeidae sp.	2	SDF[b]		X		2, 3
Ampeliscia sp.	11	SUS[b]		X	X	1, 2, 4, 5
Asteroidea						
Henricia sp.	1	P/S[b]			X	4
Anthozoa						
Gersemia rubiformis	1	SUS[b]	X			2

[a]Encyclopedia of Life (2020); [b]Macdonald et al. (2010); [c]Denisenko et al. (2015); [d]Kędra et al. (2018); [e]Divine et al. (2017)

heated at 70°C for 1 h. Hexane (4 ml) was added to the saponified solution, vortexed, and centrifuged for 3 min at 1303.4 × *g*, 3 times. The supernatant with the non-saponifiable lipids was transferred to clean glass vials and dried under a gentle N_2 stream. We removed elemental sulfur from the sediment samples following established protocols (Koch et al. 2020) to prevent analytical interference with HBI III. The initial extracts were re-suspended in hexane and fractionated using open-column silica gel chromatography. The non-polar lipids containing the HBIs were eluted, while the polar compounds were retained on the column. The eluted compounds were dried under N_2. Hexane (50 µl) was added twice to the dried purified extract and transferred to amber chromatography vials.

2.5. Biomarker analysis

The extracts were analyzed using an Agilent 7890A gas chromatograph (GC) coupled with a 5975 series mass selective detector using an Agilent HP-5ms column (30 m × 0.25 mm × 0.25 µm), following established methods (Belt et al. 2012). The oven temperature was programmed to ramp up from 40 to 300°C at 10°C min^{-1} with a 10 min isothermal period at 300°C. HBIs were identified using selective ion monitoring (SIM) techniques. The SIM chromatograms were used to quantify the HBI abundances by peak integration with ChemStation software. A purified standard of known IP_{25} concentration was used to confirm the mass spectra, retention time, and retention index (RI). The HBIs were identified by their mass ions and RI including IP_{25} (*m/z* 350.3), HBI II (*m/z* 348.3), and HBI III (*m/z* 346.3). A procedural blank was run every ninth sample. Individual HBI concentrations in the surface sediment samples were normalized by total organic carbon (TOC) on an organic gram weight basis. Surface sediment TOC data from the SWL18 and HLY18-01 cruises were accessed from the National Science Foundation's Arctic Data Center (Grebmeier & Cooper 2019b,c).

The H-Print index was used to provide an estimate of the relative organic carbon contributions of phytoplankton to sea ice algae (Brown et al. 2014c). The H-Print (Eq. 1), is calculated using the relative abundances of IP_{25}, HBI II, and HBI III, as determined from the SIM chromatograms:

$$\text{H-Print}\,\% = \frac{\text{HBI III}}{\sum(\text{IP}_{25} + \text{HBI II} + \text{HBI III})} \times 100 \quad (1)$$

The estimated organic carbon contribution varies from 0 to 100%, with lower values indicative of proportionally greater sympagic organic carbon and higher values indicative of proportionally greater pelagic organic carbon. Analytical error from replicate control tests was determined to be less than 3% for H-Print values in an individual organism from homogenized tissue sample. Sea ice organic carbon (iPOC), as a proportion of marine-origin carbon within samples, was estimated using Eq. (1) from a prior H-Print calibration from feeding experiments with known algal species ($r^2 = 0.97$, $p < 0.01$; Brown & Belt 2017):

$$\text{iPOC}\,\% = 101.08 - 1.02 \times \text{H-Print} \quad (2)$$

Given our interest in the proportion of sea ice algae utilization, the iPOC calibration is presented referenced to sea ice carbon rather than pelagic carbon, as is the case with the H-Print. However, since the calibration was derived and validated from feeding experiments, we retained the H-Print values for the sediment data. Therefore, all invertebrate samples were converted and are reported as iPOC, while sediments are reported as H-Print.

2.6. Statistical analysis

All statistical analyses were performed in R v. 3.6.1 (R Core Team 2017). Normality of the data was assessed using a Shapiro-Wilk test and the homogeneity of variance was assessed using Levene's test. We used a generalized additive model (GAM) in R using the package 'mcgv' to determine the effects of various predictor variables for the sea ice organic carbon content in benthic macrofauna. This included sea ice persistence, sampling location, feeding strategy, and sediment H-Print composition. A combination of these variables in 7 competing equations was evaluated, and the best performing equation was selected based on the lowest Akaike's information criterion (AIC) score. Linear regression models were assessed to determine the relationship between the HBI content of invertebrate tissue (iPOC%) and the corresponding surface sediment (H-Print%) they were collected from. We conducted *k*-means clustering analysis to group similar observations and assess potential patterns in the HBI distribution among location, feeding strategy, major taxa, and annual sea ice persistence. Owing to the lack of corresponding sediment samples, the samples collected from SKQ2018 (n = 41) were not included in the cluster analysis. We then used the combination of factors that explained the variation within the benthic macrofauna samples by the GAM to de-

fine the individual clusters. This analysis was conducted in R using the packages 'cluster' and 'factoextra'. Sediment H-Print and macrofauna iPOC values were normalized prior to running the cluster analysis, and the optimal number of clusters (k) was determined based on the gap statistic (Tibshirani et al. 2001). One-way ANOVA with Tukey honestly significant difference (HSD) and Bonferroni corrections were used to analyze the significant differences in relative HBI concentrations.

2.7. HBI depuration experiment

In May 2019, bivalves were collected from the pier at the Chesapeake Biological Laboratory in Solomons, Maryland, USA, using a hand-deployed PONAR grab. The 2 species collected are widely distributed and also found in parts of the Arctic: *Mya arenaria* (SUS, n = 18) and *Macoma balthica* (SUS/SDF, n = 50). *M. balthica* (n = 10) and *M. arenaria* (n = 3) were analyzed immediately (Day 0) after collection to determine their initial HBI III content from their natural environment, and the remainder (*M. arenaria*, n = 15; *M. balthica*, n = 40) were put in flow-through filtered seawater tanks (5 l). The clams were fed every other day with Shellfish Diet 1800 (Instant Algae, Reed Mariculture). The Instant Algae (1 ml) was analyzed prior to feeding to confirm there were no HBIs present.

Clams were removed from the tank, and the HBI III abundances were analyzed at 4, 7, 21, and 28 d. Owing to the small size of the individual *M. balthica* collected (~5 mm), individuals had to be grouped (n = 10 per collection date) for analysis. The *M. arenaria* samples were a sufficient size (~20–30 mm) for individual analysis (n = 3 per collection date). The relative response on the gas chromatograph-mass spectrometer (GC-MS) was recorded until the response fell below detection limits, indicating complete depuration of the biomarkers. As the depuration rate was the intended measurement, absolute quantification of HBI III was not undertaken.

3. RESULTS

Several factors were considered in various combinations to explain the variation observed in sea ice organic carbon utilization among benthic macrofauna. The GAM equation selected was based on the AIC scores, with the lowest AIC indicating the best fit. The combination of sample region, sea ice persistence, sediment H-print, and feeding strategy performed the best (AIC = 1140, $r^2 = 0.78$). Therefore, the following variables were examined in greater detail.

3.1. Surface sediment HBI distributions and relationship with sea ice

IP_{25} was only detected in trace amounts as a fraction of organic carbon (OC; <1 µg [g OC]$^{-1}$) throughout DBO 1–2 in the northern Bering Sea, and <2 µg (g OC)$^{-1}$ was observed at DBO 3 in the southern Chukchi Sea (Fig. 2A). Ledyard Bay (LB), which was only sampled for sediments, marked a transitional zone where IP_{25} levels increase in the northeast Chukchi Sea. IP_{25} reached maximum concentrations of 14.5 µg (g OC)$^{-1}$ in the northeast Chukchi Sea at DBO 4 and ranged from 1 to 10 µg (g OC)$^{-1}$ at the DBO 5 transect across Barrow Canyon. HBI III (Fig. 2B) displayed a more homogeneous distribution throughout the region. Localized areas of elevated concentrations were observed in LB, where HBI III reached 18 µg (g OC)$^{-1}$. HBI III levels were also considerably lower in the northern Bering Sea at DBO 1–2, with values ranging from 2–6 µg (g OC)$^{-1}$. H-Print (Fig. 2C) follows a latitudinal gradient from south to north with decreasing relative pelagic HBI inputs. The mean sea ice extent indicates that the IC transect was ice-covered in June but retreated by July, while the sea ice had fully retreated from DBO 4 and 5 by August.

There was a significant relationship between sea ice persistence and sediment H-Print ($r^2 = 0.61$, $p < 0.001$; Fig. 3). The DBO 1 stations experienced low (<30 d) sea ice cover in 2018 and were determined to be outliers using a Grubbs' test (Grubbs 1950) (Fig. 3). After removing the subset of DBO 1 samples (n = 3), the strength of the relationship increased, indicating a very strong fit ($r^2 = 0.81$, $p < 0.001$).

3.2. Sea ice organic carbon (iPOC%) variation by feeding strategy and region

There was an increasing gradient of sympagic utilization by benthic invertebrates from the lower latitude sampling regions (DBO 1–3) to the higher latitude sampling regions (IC and DBO 4–5; Fig. 4). The invertebrates classified as deposit feeders (both SDFs and SSDFs) generally had the highest iPOC, and SUS had the lowest within each region. The highest iPOC values were observed in the SSDF category. However, the SDFs at DBO 5 (most northerly sampling area) reached iPOC levels similar to SSDFs. The highest iPOC value observed among the SDFs at

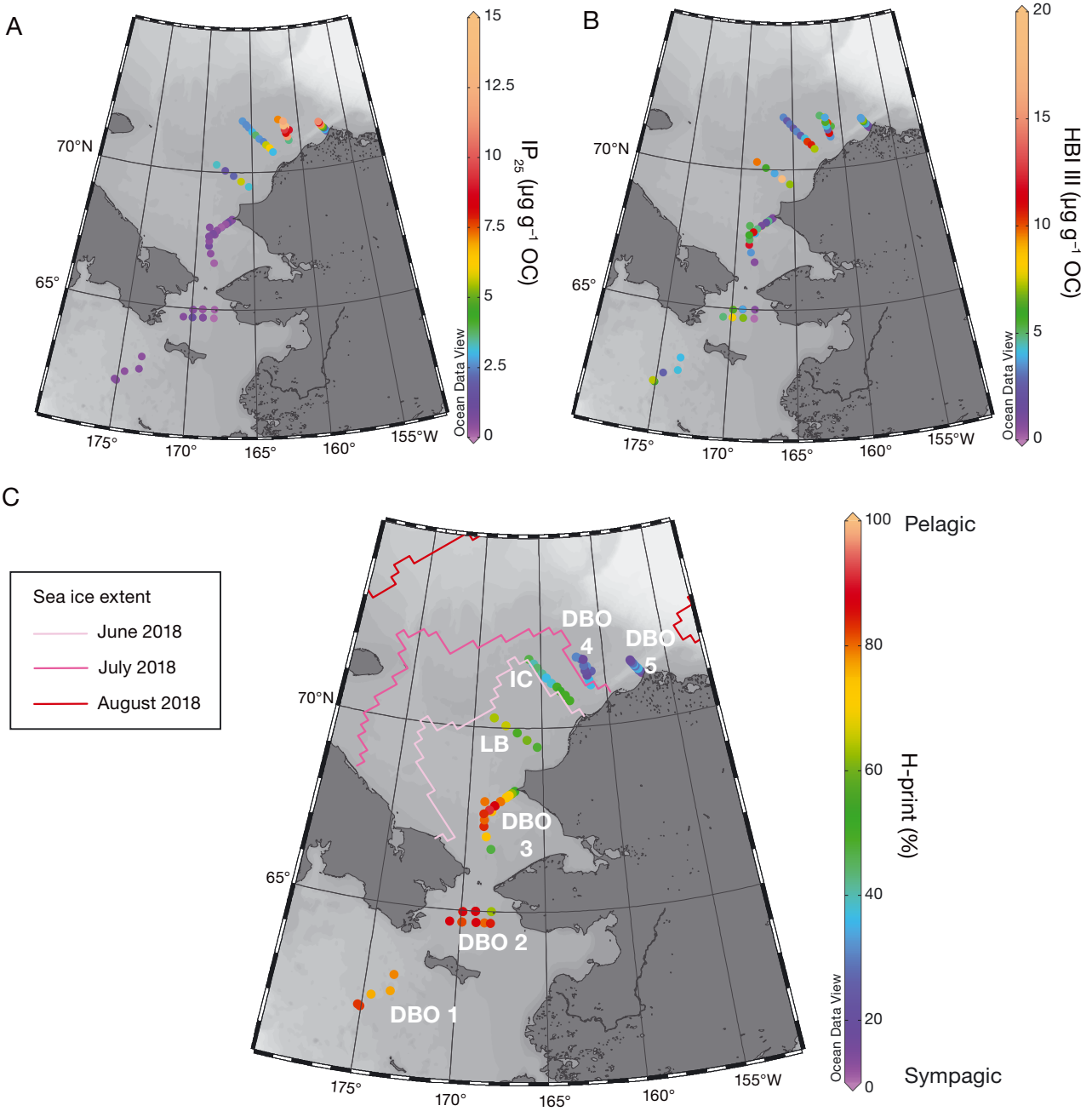

Fig. 2. Highly branched isoprenoid (HBI) biomarker analysis from surface sediments collected in July (cruise SWL18) and August (HLY18-01) in the northern Bering and Chukchi Seas. Sampling stations are shown as colored circles. (A) Distribution of the sea ice proxy IP_{25} (OC: organic carbon). (B) distribution of the pelagic HBI marker, HBI III. (C) H-Print (relative proportion of sympagic [IP_{25} and HBI II] to pelagic HBIs [HBI III]). Sample regions included Distributed Biological Observatory (DBO) 1, DBO 2, DBO 3, Ledyard Bay (LB), Icy Cape (IC), DBO 4, and DBO 5. Note: LB was only sampled for sediments and not macrofauna. The mean monthly sea ice extent is shown for June, July, and August 2018

DBO 5 (78%) was comparable to the SSDFs and attributed to sipunculids (*Golfingia margaritacea*). iPOC values increased at the IC transect. iPOC values for SUS fauna were <25% in all sampling regions, with the exception of DBO 4, indicating that they were utilizing predominantly pelagic resources. P/Ss by comparison had a less clear trophic dependence on sympagic sources relative to the other feeding strategies from DBO 1–3. The SUS/SDFs aligned with SUSs but with greater differences at IC and DBO 5. Feeding strategies were significantly different ($p < 0.05$) at all stations except DBO 1 and 2, as determined by 1-way

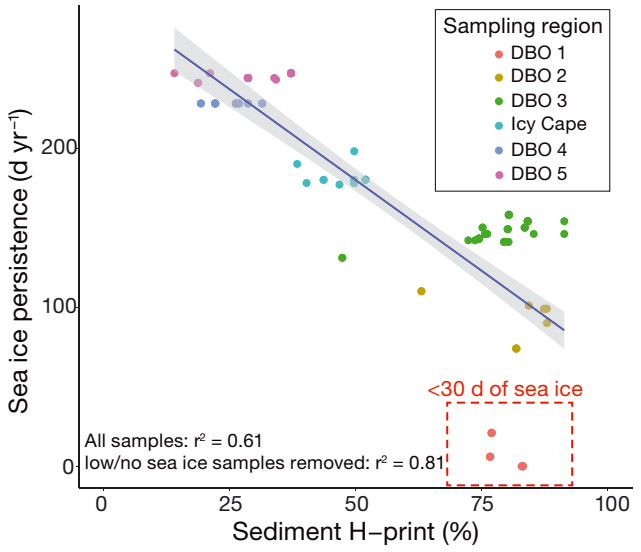

Fig. 3. Linear regression with 95% confidence interval (shaded region) of sea ice persistence and sediment H-Print (see Fig. 2 for definition). Colors indicate the Distributed Biological Observatory (DBO) sampling regions (see Fig. 2 for locations). The no/low sea ice stations were deemed outliers, and the corresponding r^2 values with and without these outliers are shown

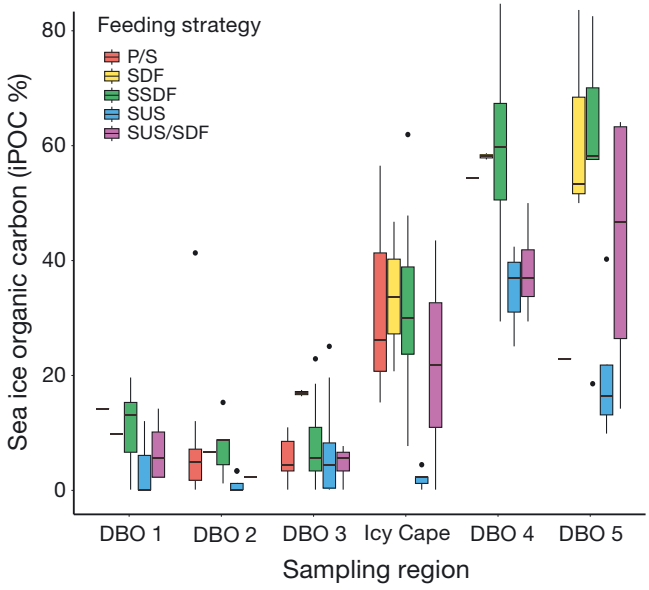

Fig. 4. Sea ice organic carbon (iPOC) by feeding strategy across the Distributed Biological Observatory (DBO) sampling regions in 2018. Feeding strategies include: predator/scavenger (P/S), suspension feeder (SUS), surface deposit feeder (SDF), subsurface deposit feeder (SSDF), and suspension/surface deposit feeder (SUS/SDF). Sample regions from south to north included DBO 1, DBO 2, DBO 3, Icy Cape, DBO 4, and DBO 5 (see Fig. 2 for locations). The boxes indicate the interquartile range from the first to third quartiles, with the median shown as the line within each box. The minimum and maximum are indicated by the lines, and outliers are shown as individual points

ANOVA (Table 3). Tukey HSD pairwise comparisons indicated that SUS were significantly different from SDFs and SSDFs at all 4 of these sampling regions (see Table S1 in the Supplement at www.int-res.com/articles/suppl/m651p023_supp.pdf for p-values).

3.3. Relationships between macrofauna iPOC and sediment H-Print

The linear regression of normalized iPOC values for the invertebrate tissues and corresponding H-Print values in surface sediments indicates a significant relationship between these variables ($p < 0.001$, $r^2 = 0.66$). The samples were grouped into 3 clusters (Fig. 5A). The cluster composition took advantage of the prior assessments of the factors determined to be significant (e.g. DBO region and feeding strategy; Fig. 5B,C). Sea ice persistence patterns and taxa composition were also examined for each of the clusters.

Cluster 1 samples were found throughout the Chukchi Sea, including DBO 3, DBO 4, DBO 5 and IC (Fig. 5B), with a majority (52%) from IC (Table 4). The difference in feeding strategy was not significant based on a 1-way ANOVA (Table 3). The composition of feeding strategies contained in cluster 1 (Fig. 5C) was distributed among SUSs (38%), SSDFs (28%), SUS/SDFs (17%), SDFs (3%), and P/Ss (14%; Table 4). The SSDF group had the highest mean (±SD) iPOC (23 ± 9%) and SUSs had the lowest (10 ± 9%; Fig. S1). This cluster was dominated by bivalves (62%) and polychaete worms (21%). Overall, cluster 1 had a moderate sediment H-Print (42 ± 11%) with invertebrate iPOC values indicative of low sea ice organic carbon utilization (mean iPOC: 17 ± 10%; Table 4). The mean sea ice persistence for this cluster was 205 ± 35 d (Table 4).

Cluster 2 stations were located in the northeast Chukchi Sea from IC, DBO 4, and DBO 5 (Fig. 5B), with the majority from DBO 4 (66%; Table 4). The organisms sampled in this cluster were predominantly SSDFs (57%; Table 4). Two of the 3 SUS samples included in this cluster (bivalve *Astarte borealis* and amphipod *Ampeliscia* sp.) were from a station in DBO 4 with high IP_{25} deposition (DBO 4.4). Feeding strategy was significant based on the 1-way ANOVA ($p < 0.05$; Table 3). The iPOC values in this cluster were highest overall. Values ranged from 37–57%, with SSDFs having the highest (57 ± 11%), and SUS/SDFs the lowest (37 ± 3%; Fig. S1). The Tukey HSD pairwise comparison indicated that SUS/SDF–SSDF and SUS–SSDF were significantly different ($p < 0.05$; Table S1). Cluster 2 contained bivalves (52%) and

Table 3. ANOVA results for H-Print (defined in Fig. 2) for each of the Distributed Biological Observatory (DBO) regions and clusters (see Fig. 5). Significance is denoted as $^{*}p < 0.05$, $^{**}p < 0.01$, $^{***}p < 0.001$ (p-adj: adjusted p-value)

Group	Factor	df	SS	MS	*F*	p-adj
DBO 1	Feeding strategy	4	113.4	28.36	0.70	0.612
	Residuals	9	365.4	40.60		
DBO 2	Feeding strategy	4	302.7	75.66	1.51	0.23
	Residuals	25	1252.7	50.11		
DBO 3	Feeding strategy	4	267.9	66.98	2.72	0.0358*
	Residuals	73	1796.5	24.61		
Icy Cape	Feeding strategy	4	2898.0	724.60	3.08	0.049*
	Residuals	15	3534.0	235.60		
DBO 4	Feeding strategy	4	2657.0	664.30	5.46	0.002**
	Residuals	27	3288.0	121.80		
DBO 5	Feeding strategy	4	4645.0	1161.30	3.47	0.036*
	Residuals	14	4680.0	334.30		
Cluster 1	Feeding strategy	4	847.8	211.95	2.36	0.0818
	Residuals	24	2154.0	89.75		
Cluster 2	Feeding strategy	4	1814.0	453.40	3.93	0.009**
	Residuals	39	4501.0	115.40		
Cluster 3	Feeding strategy	4	521.5	130.40	7.76	<0.001***
	Residuals	70	1176.2	16.80		

polychaete worms (25%), but also an increased contribution from sipunculids (9%; Table 4). The mean sediment H-Print was low (i.e. sympagic) at 29 ± 7%, with invertebrate iPOC values ranging from moderate to high with a mean value of 53 ± 12% (Table 4). The mean sea ice persistence was the longest of all clusters at 227 ± 18 d of the year (Table 4).

Cluster 3 contained the northern Bering Sea (DBO 1 and 2) and southeast Chukchi Sea (DBO 3) stations, immediately north and south of Bering Strait (Fig. 5B). Cluster 3 contained all the samples from DBO 1 and 2, but 63% of the samples comprising the cluster were from DBO 3 (Table 4). Feeding strategy was a significant variable for this cluster based on 1-way ANOVA ($p < 0.001$; Table 3). SUS (27%), SSDF (35%), and SUS/SDF (27%) were the primary feeding strategies within this cluster (Table 4). SDFs had the highest mean iPOC value (13 ± 6%), and SUSs the lowest at 1 ± 3%, meaning food sources were nearly completely pelagic (Fig. S1). The differences were significant between SUS–P/S ($p < 0.05$), SUS–SDF ($p < 0.01$), and SUS–SSDF ($p < 0.001$) based on pairwise comparisons (Table S1). Cluster 3 was dominated by bivalves (52%) and polychaetes (27%), with an increased contribution from ampeliscid amphipods (13%; Table 4). The mean sediment H-Print was high (80 ± 5%, i.e. pelagic), and the mean iPOC value in invertebrate tissues was low (5 ± 5%; Table 4). The sea ice persistence for cluster 3 was the shortest at 111 ± 55 d (Table 4).

3.4. Sea ice persistence and sea ice organic carbon (iPOC%)

The clusters were further analyzed using the linear regression of sea ice persistence determined from each of the sampling locations relative to the invertebrate tissue iPOC (Fig. 6A). The clusters remained distinctly grouped with the exception of 2 data points from cluster 1. The relationship between sea ice persistence and sea ice carbon utilization was significant ($p < 0.001$, $r^2 = 0.41$; Fig. 6A). However, there was a distinct group from cluster 3 with stations that experienced less than 30 d of sea ice, including several samples where there was no sea ice cover in 2018 (Fig. 6A). By removing this cluster from the linear regression, the fit of the relationship improved ($r^2 = 0.56$, $p < 0.001$). All stations with no or low sea ice cover occurred at DBO 1, also known as the St. Lawrence Island polynya (SLIP) region (Fig. 6B). Stations SLIP 1 and SLIP 2 had no sea ice cover during the study period in 2017–2018, while SLIP 3 and SLIP 5 had less than 30 d of sea ice. The SDF and SUS/SDF iPOC were lowest at SLIP 1 and 2, with values at or near 0%. The SSDF and P/S iPOC values were slightly higher, but still consistent with dominantly pelagic organic carbon acquisition (<20% sea ice organic carbon). The patterns were less clear at SLIP 3 and 5, with both SSDF and SUS sea ice organic carbon sources <10% and a group of SSDF, SDF, and SUS/SDF falling between 6 and 18% (Fig. 6B).

3.5. Sea ice organic carbon (iPOC%) utilization by major taxa

The species that contained the highest iPOC values (>75%) included maldanid polychaetes, the sipunculid *Golfingia margaritacae*, and the clam *Ennucula tenuis* (Fig. 7A). High levels of iPOC (50–75%) were observed in the clams *Yoldia hyperborea* and *Macoma calcarea*, brittle star *Ophiura sarsii*, polychaete *Pectinaria hyperborea*, amphipod family Lysianassidae (not practical to identify species at sea), and sea star *Henricia* sp. Moderate iPOC levels (25–50%) were observed in the clams *Nuculana pernula* and *Astarte borealis*, the gastropod *Buccinum scalariforme*, and the amphipod *Ampeliscia* sp. The lowest iPOC levels (<25%) occurred in the snow crab *Chio-*

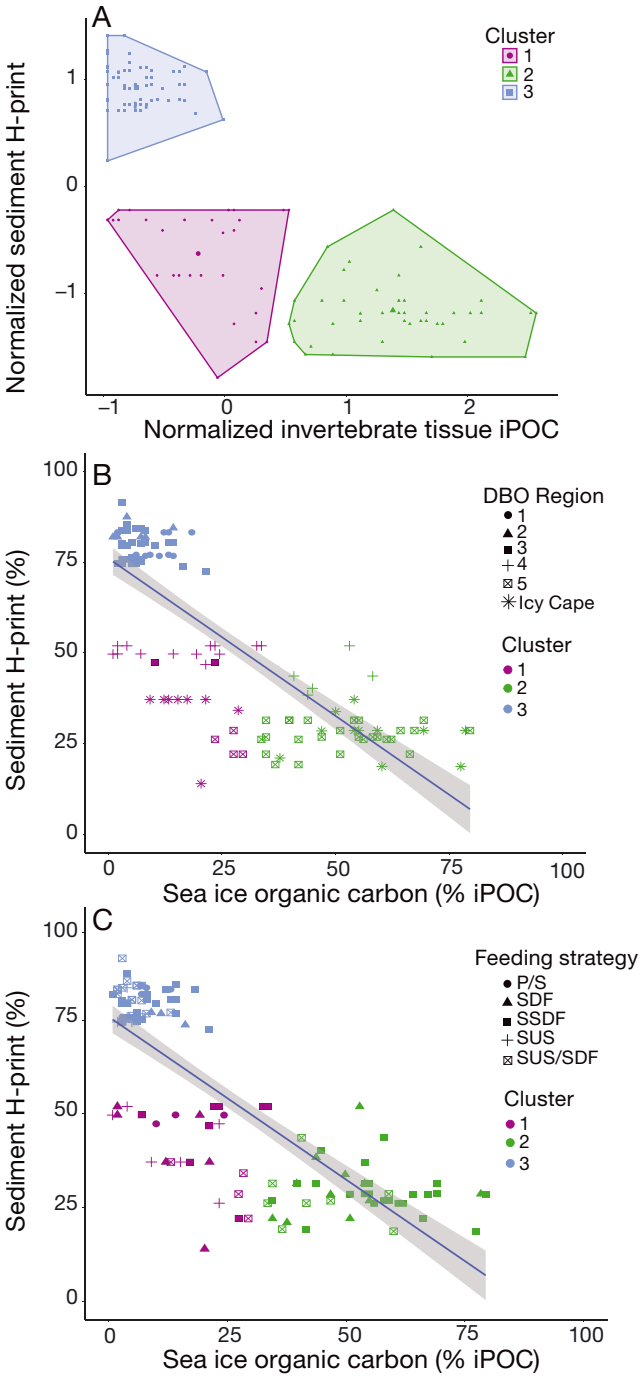

Fig. 5. Results of the *k*-means clustering analysis between macrofaunal tissue and the sediment from which the organisms were collected. (A) Normalized sediment H-print (see Fig. 2 for definition) and macrofauna tissue percentage of sea ice organic carbon (iPOC) values grouped into the optimal number of clusters (n = 3). (B) Sediment H-Print and macrofaunal tissue iPOC, with symbols represented by Distributed Biological Observatory (DBO) sampling region and colors representing cluster number. (C) Sediment H-Print and invertebrate tissue iPOC, with symbols representing feeding strategy (defined in Table 2) and colors representing cluster number. Linear regressions in (B) and (C) are shown with 95% confidence intervals (shaded region)

noecetes opilio, the predatory polychaete *Nephtys* sp., the bivalves *Serripes laperousii* and *Mya* sp., and all tunicates, holothuroids, ascidians, anthozoans, and the remaining gastropods. Estimates of iPOC by feeding strategy (Fig. 7B) revealed a dominance of SSDFs in the utilization of sea ice organic carbon (iPOC >50%). The SDF organisms were primarily in the moderate to high range of iPOC, but also contained the highest mean iPOC values (e.g. sipunculids and brittle stars). None of the SUSs exceeded use of more than 25% sea ice carbon.

3.6. HBI depuration rates

The depuration rates determined from the temperate clam experiment suggested similar timing for SUS/SDF *Macoma balthica* and SUS *Mya arenaria* at 21 and 28 d, respectively (Fig. 8). Relative HBI III abundance indicated reductions by Day 7 in both species; however, there were detectable levels until the 3 to 4 wk sampling events.

4. DISCUSSION

4.1. HBI distributions in surface sediments

The spatial distribution of H-Print in surface sediments in 2018 (Fig. 2C) followed a latitudinal gradient previously observed for the region (Koch et al. 2020). IP_{25} concentrations were relatively high in surface sediments in the northeast Chukchi Sea compared to previous years, exceeding 14 µg $(g\ OC)^{-1}$ (Fig. 2A). The strong relationship between sea ice persistence and sediment H-Print supports the use of these biomarkers in this region as diagnostic of sea ice cover (Fig. 3). Based on the distribution of HBIs, we hypothesized that the invertebrate HBI composition would be influenced by the regional HBI patterns in the surface sediments as indicators of available food sources. Linear regressions between sediment H-Print and macrofaunal iPOC confirmed that location was a significant influence (Figs. 4 & 5C).

4.2. Influence of sea ice persistence on cluster composition

Sea ice persistence, which was correlated with DBO region, appeared to be an important factor in the cluster analysis. The samples in cluster 3 were located in the 3 southern DBO regions (Table 4,

Table 4. Summary parameters for the *k*-means clustering analysis including the cluster composition by Distributed Biological Observatory (DBO) region (see Fig. 1; IC: Icy Cape), feeding strategy (see Table 2 for definitions) and dominant taxa, mean sediment H-Print (%; defined in Fig. 2), mean macrofaunal tissue sea ice organic carbon (iPOC%), and mean sea ice persistence (± values are SD). Dashes for DBO region indicate there were no samples from those regions in that particular cluster

	Cluster composition						Mean sediment H-print	Mean sea ice carbon (iPOC%)	Mean sea ice persistence (d)
	DBO region (%)		Feeding strategy (%)		Dominant taxa (%)				
Cluster 1	1	–	SUS	38	Bivalvia	62	Mixed composition		
(n = 29)	2	–	SSDF	28	Polychaeta	21	42 ± 11	17 ± 10	205 ± 35
	3	7	SUS/SDF	17					
	IC	52	SDF	3					
	4	14	P/S	14					
	5	28							
Cluster 2	1	–	SUS	7	Bivalvia	52	Sympagic		
(n = 44)	2	–	SSDF	57	Polychaeta	25	29 ± 7	53 ± 12	227 ± 18
	3	–	SUS/SDF	18	Sipuncula	9			
	IC	6	SDF	14					
	4	66	P/S	5					
	5	25							
Cluster 3	1	19	SUS	27	Bivalvia	52	Pelagic		
(n = 75)	2	19	SSDF	35	Polychaeta	27	80 ± 5	5 ± 5	111 ± 55
	3	63	SUS/SDF	27	Ampeliscidae	13			
	IC	–	SDF	3					
	4	–	P/S	9					
	5	–							

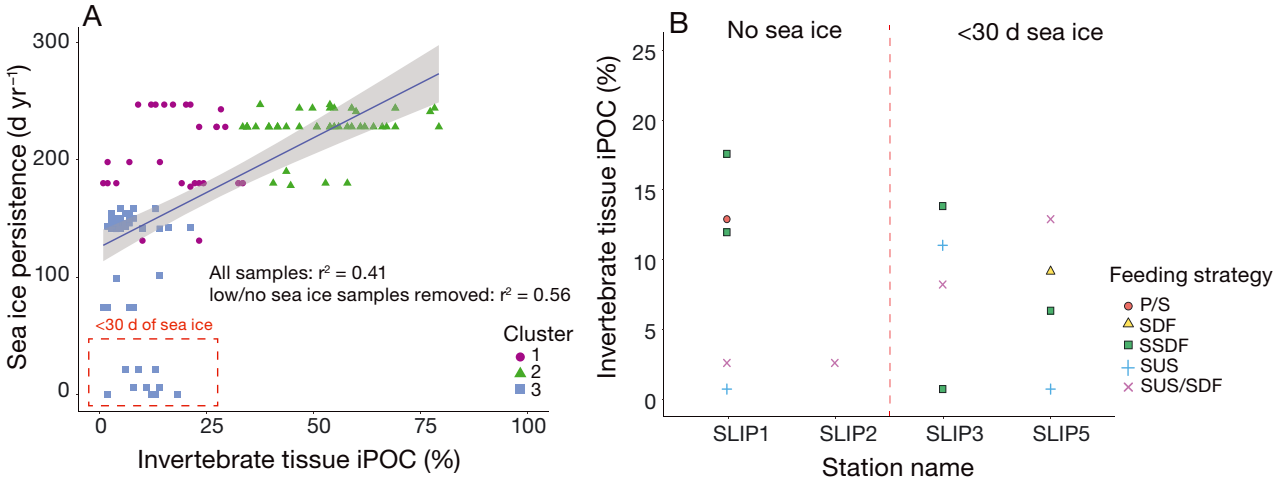

Fig. 6. (A) Linear regression of sea ice persistence and macrofauna sea ice organic carbon (iPOC). Clusters are represented by corresponding shape/color. The samples that were deemed outliers due to low sea ice persistence or no sea ice cover in 2018 are enclosed in the dashed-red box. The linear regression is shown with a 95% confidence interval (shaded region). (B) Macrofaunal tissue iPOC% from the no/low sea ice group by station in the DBO 1/St. Lawrence Island Polynya (SLIP) region. Symbols and corresponding colors represent feeding strategies (defined in Table 2) of individual samples at these locations

Fig. 5). Baseline studies of H-Print in Pacific Arctic surface sediments suggest that a dominance of pelagic carbon is common throughout these 3 DBO regions (Koch et al. 2020). However, a defining feature of this region in 2017–2018 was the record low maximum sea ice extent (Grebmeier et al. 2018, Stabeno & Bell 2019). This may be the reason for the outlier iPOC signatures from benthic macrofauna samples collected at SLIP 1 and SLIP 2, where there was no sea ice cover and presumably no freshly deposited ice algae (Fig. 6). The large ice-edge bloom that typically occurs in April or May over the northern Bering shelf

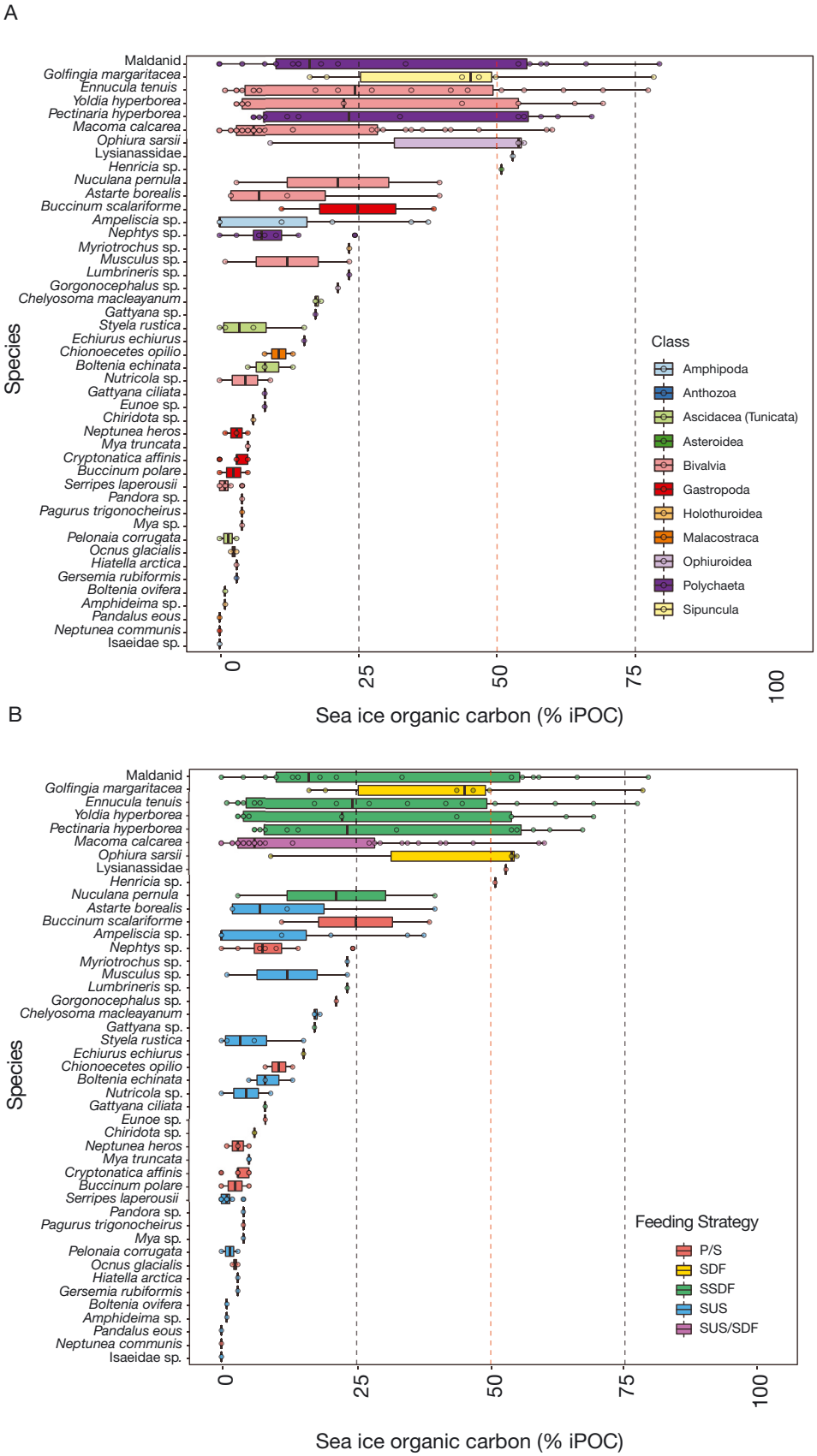

Fig. 7. Sea ice organic carbon (iPOC) composition by species and shown by (A) major taxa and (B) feeding strategy. See Fig. 3 for boxplot descriptions and Table 2 for feeding strategies. Shaded points represent individual samples

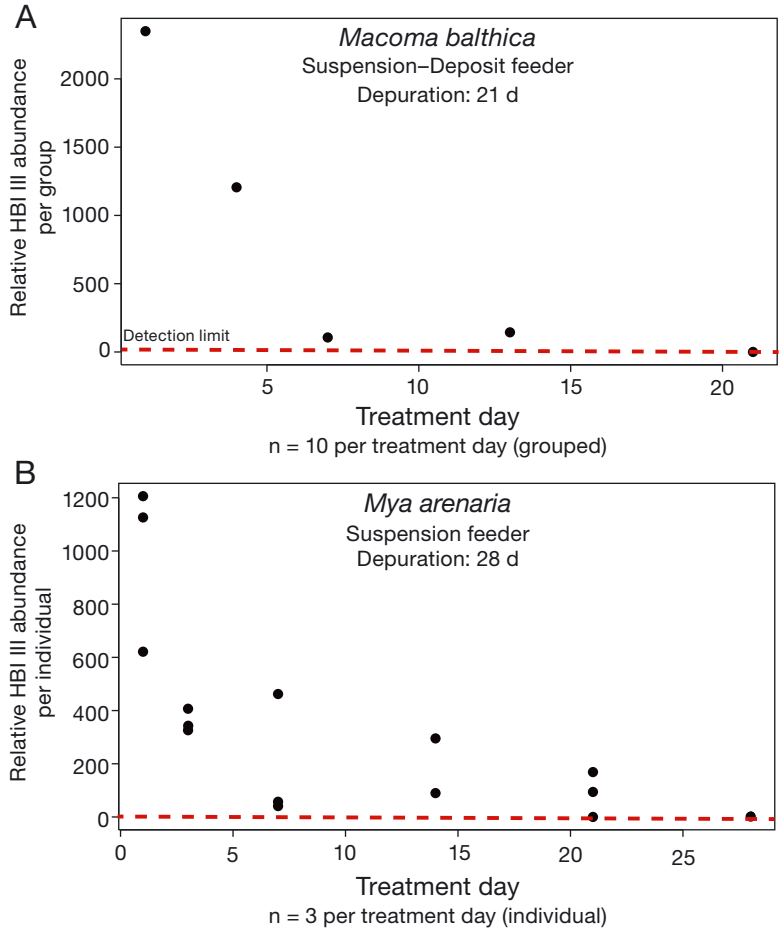

Fig. 8. Experimental highly branched isoprenoid (HBI) III depuration rates in temperate clam samples. (A) Suspension–surface deposit feeding *Macoma balthica.* Individual points represent n = 10 clams. (B) suspension feeding *Mya arenaria*. Individual points represent n = 1 clam. The red-dashed line indicates the GC-MS detection limit for HBIs

did not occur in 2018, according to primary production measurements derived from satellite observations of chlorophyll *a* (Frey et al. 2018). The late pelagic bloom and abnormally low chlorophyll in the northern Bering Sea near DBO 1 were observed from fluorescence sensors on the M5 mooring (Duffy-Anderson et al. 2019). The lack of sea ice also led to bottom water temperatures that were above 0°C for the first time since observations began in 1988 (Grebmeier & Cooper 1995, Grebmeier et al. 2018), eliminating the cold pool that typically serves as a thermal barrier to several pelagic and demersal fish species that could alter benthic food webs (Grebmeier et al. 2018, Duffy-Anderson et al. 2019). An observed ecosystem shift in this region has occurred over the last few decades, including a northward shift in benthic biomass and decline of nuculanid and nuculid bivalves replaced by maldanid polychaetes (Grebmeier et al. 2006b, 2018). There has also been a northward contraction of the bivalve *Macoma calcarea* within the sampled stations in DBO 1 (Goethel et al. 2019). A recent study concluded that physical oceanographic shifts in this system are largely responsible for driving the changes seen in benthic community structure (Waga et al. 2020), and it seems plausible that these shifts are likely connected to changing food sources in the northern Bering Sea.

Moving northward, cluster 1 had a majority of the IC samples and a subset of samples from DBO 5 (Table 4, Fig. 5). The IC transect was located at the approximate position of the ice-edge through June and July before the rapid retreat off of the Chukchi shelf by August (Fig. 2C). At this location, the ice retreats in an onshore to offshore pattern with sea ice persistence lower by 20–30 d at the onshore sampling locations. This transect is also located at the start of the Central Channel for Bering Sea water transport northwards, and current flow increases, as indicated by coarser grain sizes (Grebmeier & Cooper 2019c), suggesting reduced deposition of particulate organic matter including ice algae and phytoplankton. The sea ice persistence patterns, location of the mean ice edge for June and July, and sediment H-Print values show a clear delineation between IC and DBO 4 despite their relatively close proximity (Figs. 1 & 2). There is also a front that forms between these regions, keeping warmer, nutrient-poor Alaska coastal water south and offshore and nutrient-rich Bering Sea water to the north near DBO 4 (Weingartner et al. 2017). The strong negative correlation between sea ice persistence and H-Prints suggest that the additional approximate month of sea ice at DBO 4 driven by the hydrography had an impact on IP_{25} synthesis and deposition. The SDFs at IC also contributed to the elevated iPOC values associated with this cluster (Fig. 4). The DBO 5 line is a transect across Barrow Canyon. The H-Prints are elevated in the center of the canyon (~35%), yet still dominantly sympagic, and decrease on the sides (~14–18%). We attribute this cross-sectional pattern to the flow through Barrow Canyon, where currents converge with mean speeds of 15–20 cm s^{-1} (Bering water) and surface

currents upwards of 70–100 cm s^{-1} (Alaska Coastal Current on the eastern flanks) with bottom intensified flows (Aagaard & Roach 1990, Pickart et al. 2005, 2019). Although Barrow Canyon is on the northeast Chukchi Shelf where ice algae influence is most significant, ice algal aggregates likely do not settle to the bottom of Barrow Canyon as readily because of stronger currents than on the shelf, and organic materials are transported towards the basin because of these enhanced current speeds (Lepore et al. 2009). Additionally, the high current speeds in Barrow Canyon favor suspension over deposit feeding (Pisareva et al. 2015). Therefore, the reason for these DBO 5 samples to be clustered with IC is likely due to the apparent increased phytoplankton utilization by SUSs relative to DBO 4 (Fig. 4).

As previously noted, DBO 4 and 5 dominated the cluster 2 composition in the northeast Chukchi Sea where ice algae deposition and utilization were most substantial. Fewer SUSs and P/Ss were collected within the offshore DBO 4 transect. Macrofaunal biomass at these sites is typically dominated by deposit feeders, primarily sipunculids and maldanid polychaetes, but also brittle stars (Ophiuridae) and bivalves (Yoldiidae and Astartidae) and occasionally the SUS/SDF bivalve *M. calcarea* (Grebmeier & Cooper 2019a). Depositional regimes on the Chukchi shelf, such as along DBO 4, tend to favor deposit feeders over SUSs (Pisareva et al. 2015). The HBI data show that the pairing of longer sea ice persistence in a depositional environment results in higher ice algae utilization. Recent studies indicated that IP_{25} and diatom export occur year-round at this location (Koch et al. 2020, Lalande et al. 2020). There is currently a lack of HBI flux data available from other DBO regions, but preliminary HBI data from sediment traps at DBO 2 and DBO 3 suggest that this steady supply of sympagic HBIs is likely a unique feature at DBO 4 (C. W. Koch unpublished data). Although pelagic phytoplankton blooms are greater in the summer as seasonal ice retreats, in addition to the occurrence of under-ice phytoplankton blooms (Arrigo et al. 2014, Assmy et al. 2017), the continuous export of IP_{25} suggests that a sustained source of sea ice carbon is transported to the benthos, both when grazing pressure in the water column is minimal and as a result of re-suspension events throughout the year (Koch et al. 2020). The mean iPOC value in the invertebrate tissue samples suggests an approximate 50:50 mixture of ice algae and phytoplankton, although our analysis does not preclude organic carbon from other possible detrital or terrestrial sources. Feeding experiments providing both ice algae and phytoplankton to benthic consumers have shown that certain organisms may preferentially consume ice algae (McMahon et al. 2006, Sun et al. 2009). It has also been suggested that despite the preference for ice algae, many Arctic macrofauna exhibit dietary plasticity and will respond similarly to availability of either category of organic matter and may not be dependent on ice algae (Mäkelä et al. 2017, Kędra et al. 2019).

4.3. Sea ice carbon utilization by feeding strategy

Location did not fully account for the variability among the sampled organisms and was the basis for exploring the differences among species and feeding strategies. Deposit feeders have been previously observed to have greater ice algae utilization than SUSs based upon fatty acid concentrations in macrofaunal tissues in the Chukchi Sea (Schollmeier et al. 2018). This was similarly demonstrated through feeding experiments and was attributed to preferential grazing on the higher fatty acid composition of ice algae (McMahon et al. 2006). Our iPOC measurements confirm these findings, with higher values for SDFs and SSDFs than SUSs throughout the study area (Fig. 4). Our HBI measurements do not mean that SUSs do not utilize ice algae from the water column. However, because ice algae aggregates sink rapidly to the seafloor and can overwhelm any pelagic grazers present, it is possible that much of the ice algae is not immediately consumed but is incorporated into the surface sediments (Legendre et al. 1992). By contrast, SUSs may more predominantly depend on water column phytoplankton that can be suspended in the water column over longer periods of the seasonal cycle.

Understanding HBI retention in consumers is critical to fully interpreting any transition in food sources as sea ice coverage diminishes. Short residence times (days to weeks) of HBIs in various consumer tissues have been suggested from previous studies (Brown & Belt 2012, Brown et al. 2013, 2014a). Based on the results from the HBI III depuration experiment (Fig. 8), and the assumption that those temperate results are generalizable to higher latitudes, the HBI signal may represent assimilation over the course of approximately 1 mo prior to sampling. Similar assimilation rates (i.e. approximately 1 mo) of organic carbon were determined in Arctic bivalves using isotope-labeled ice algae (McMahon et al. 2006). While IP_{25}-specific depuration rates are currently unavailable, a starting point might be to assume that this compound would behave similarly to HBI III, with further exper-

imentation required to confirm this. Complexities include prior studies which suggested that metabolic rates can be quite variable in response to seasonal variations in temperature (Jansen et al. 2007) or that Arctic bivalves use elevated metabolic rates at low temperatures as an adaptation strategy (Thyrring et al. 2015). The potential influence of temperature on metabolic rates when comparing our experiment using temperate species with Arctic species clearly imposes some limitations on the extent of possible interpretation. However, the results of this experiment demonstrate that very short lipid depuration (i.e. less than 48 h) or bioaccumulation were not observed. If either were to be the case, relationships between sea ice and organic carbon transfer to higher trophic levels would be more ambiguous to interpret.

Ice algae deposition occurred with the shortest time interval in the northeast Chukchi Sea stations prior to sampling, allowing for the freshest deposition of iPOC at those locations. Owing to the low sea ice conditions in the Bering Strait region in 2018, there would have been little to no opportunity for ice-associated blooms, as was evident in the anomalous timing of maximum chlorophyll biomass in June rather than April–May (Frey et al. 2018). Therefore, the low levels of iPOC in deposit feeders from DBO 1 and 2 (Fig. 6B) were most likely from previous years' sea ice carbon stored in the sediments. This indicates that this carbon source may serve as a reserve of lipid-rich organic matter in low sea ice years. This 'sediment food bank' on polar shelves has been supported by other studies (Mincks et al. 2005, Pirtle-Levy et al. 2009, Sun et al. 2009, McTigue & Dunton 2014, North et al. 2014, Schollmeier et al. 2018). Analysis of HBIs from sediment cores on the Chukchi Shelf indicate that IP_{25} is well-mixed by bioturbation and can increase with depth (Koch et al. 2020). However, biological utilization of stored sea ice carbon and consistent burial through bioturbation will ultimately deplete these reserves, and subsequently the associated sympagic HBIs.

The importance of ice algae to P/Ss is not clear in light of our results. The iPOC values of these organisms suggest that ice algae may not be a significant component of their diet, which indicates more about their available prey items. It appears that P/Ss had comparable sea ice organic carbon levels to deposit feeders at IC (Fig. 4). Unfortunately, our sample sizes at DBO 4 and 5 were too low to robustly investigate this relationship where ice algae are incorporated into tissues in greater proportions. Future studies focused in these locations to analyze the progression of iPOC values in P/Ss and their preferred prey following sea ice retreat would be useful to better understand the significance of ice algae sources to these organisms, as they serve as important trophic links in the Pacific Arctic food web (Bluhm et al. 2009).

The SUS/SDF tellinid clams (e.g. *M. calcarea*) had a wide range of iPOC values. *M. calcarea* are found throughout the Pacific Arctic region and often dominate the macrofaunal biomass (Grebmeier et al. 2018). Their dietary plasticity is advantageous to allow for broader utilization of the available food source. The ranges of iPOC values of *M. calcarea* were between those of the deposit feeders and SUSs, suggesting utilization of dual feeding strategies. Prior work found that *Macoma* species preferred ice algae over phytoplankton (Sun et al. 2009), but compound-specific stable isotope analysis of amino acids has also revealed that some deposit feeding benthic species with high feeding plasticity can adjust feeding strategies in response to the quality and availability of organic matter reaching the seafloor (Kędra et al. 2019). One other species in this study, *Golfingia margaritacea* (Sipuncula), is primarily a deposit feeder in the Pacific Arctic but is also capable of suspension feeding (Gibbs 1977, Kędra et al. 2018). Sipunculids may utilize this feeding method in high current flow regions like that of Barrow Canyon where sipunculan abundance is high (Kędra et al. 2018).

4.4. Elevated sea ice carbon utilization in select Pacific Arctic benthic macrofauna

G. margaritacea was 1 of 2 species in which the low end of the interquartile range of iPOC values was in the moderate utilization category for ice algae (25–50%, Fig. 7B). It also had one of the highest mean iPOC values overall. This range of iPOC values suggests that *G. margaritacea* is one of the benthic macrofaunal groups most reliant on ice algae in the Pacific Arctic. *G. margaritacea* abundance is greater in the Chukchi Sea than in the northern Bering Sea, particularly in depositional environments, which may be driven by sea ice persistence and differing food types reaching the seafloor (Kędra et al. 2018). Our results also suggest there may be an association between ice algae deposition and sipunculan distributions. Sipunculids are a known prey item for important higher trophic organisms including the Pacific walrus (Sheffield & Grebmeier 2009, Jay et al. 2014), snow crab (Divine et al. 2017), and possibly others (Kędra et al. 2018). We also found that the brittle star *Ophiura sarsii* had elevated sea ice algae depend-

ence relative to other species. Elevated ice algae utilization by ophiuroids has been observed in the Canadian Arctic using HBIs, stable isotopes, and fatty acids (Kohlbach et al. 2019). *O. sarsii* are widely distributed throughout the Pacific Arctic; however, they are most abundant in the northern Chukchi Sea compared to the south (Ambrose et al. 2001, Bluhm et al. 2009), although they are also abundant in the muddy sediments on the outer shelf-slope southwest of St. Lawrence Island (Grebmeier et al. 2015). Brittle star abundance is associated with finer grain sizes (Grebmeier et al. 2015), but our HBI data suggest that it could also be influenced by the availability of ice algae as a food source in these depositional environments. *O. sarsii* are also a prey item for snow crabs in addition to sea stars and buccinid snails (Bluhm et al. 2009), which are similarly important trophic links to marine mammals. Despite the suggestion of potential plasticity to food quality and availability, based upon biomarker evidence, sipunculids and brittle stars seem to have a preference for ice algae and may face greater impacts from shifting food sources as seasonal sea ice coverage is reduced.

5. CONCLUSIONS

The main goal of this study was to determine the relative importance of ice algae on the highly productive shelves of the Pacific Arctic. The detection of sea ice source-specific biomarkers IP_{25} and HBI II, in comparison to the pelagic-sourced HBI III biomarker, suggests that both SDFs and SSDFs in this region are more reliant on ice algae, compared to SUSs and P/Ss. Sea ice carbon is more abundant and utilized in greater proportions in the northeast Chukchi Sea relative to the northern Bering Sea and Bering Strait regions to the south. Our findings indicate that benthic communities of the Pacific Arctic display dietary plasticity for both sea ice and pelagic food sources, with elevated ice algae utilization across several taxa and feeding strategies, either driven by elevated lipid content or by availability and accessibility of this food source. Changes in quality, quantity, and timing of primary production are likely to impact these benthic populations. The concept of a food bank stored within sediments on Arctic shelves is further supported here. This reservoir of organic matter may provide prolonged access to lipid reserves in the sediment in low sea ice years and in the decades to come. If ice algae production becomes much less prominent as the ice edge retreats northward, the sympagic carbon reserves in sediments will eventually be depleted and replaced by exclusively pelagic-sourced carbon, which may particularly affect those organisms that currently obtain nearly half of their carbon from ice algae. The incorporation of HBI measurements into Arctic benthic food web studies provides advantages as a monitoring tool because of the source-specificity associated with the sea ice origin of organic matter. While the HBI measurements improve our ability to track the utilization of sea ice primary production, they may not fully capture the pelagic primary production and might be best considered complementary measurements to other diagnostic analyses such as stable isotopes and essential fatty acids.

Acknowledgements. We thank the captains and crews aboard the CCGS 'Sir Wilfrid Laurier' and USCGC 'Healy'. We also thank Katrin Iken (University of Alaska Fairbanks) for epibenthic sample collection and identification from the ASGARD cruise on the RV 'Sikuliaq'. We thank the 4 anonymous reviewers for their constructive comments that helped improve an earlier version of the manuscript. Financial support was provided by grants from the US National Science Foundation Arctic Observing Network program (Award 1917469 to J.M.G. and L.W.C. and Award 1917434 to K.F.) and NOAA Arctic Research Program (CINAR 22309.07) to J.M.G. and L.W.C. We thank the North Pacific Research Board (NPRB) for additional funding support provided to C.W.K. through the NPRB Graduate Research Award.

LITERATURE CITED

Aagaard K, Roach A (1990) Arctic ocean-shelf exchange: measurements in Barrow Canyon. J Geophys Res Oceans 95:18163–18175

Ambrose W, Clough L, Tilney P, Beer L (2001) Role of echinoderms in benthic remineralization in the Chukchi Sea. Mar Biol 139:937–949

Amiraux R, Smik L, Köseoğlu D, Rontani JF and others (2019) Temporal evolution of IP_{25} and other highly branched isoprenoid lipids in sea ice and the underlying water column during an Arctic melting season. Elem Sci Anth 7:38

Arrigo KR (2014) Sea ice ecosystems. Annu Rev Mar Sci 6: 439–467

Arrigo KR, van Dijken GL (2015) Continued increases in Arctic Ocean primary production. Prog Oceanogr 136:60–70

Arrigo KR, Perovich DK, Pickart RS, Brown ZW and others (2014) Phytoplankton blooms beneath the sea ice in the Chukchi sea. Deep Sea Res II 105:1–16

Assmy P, Fernández-Méndez M, Duarte P, Meyer A and others (2017) Leads in Arctic pack ice enable early phytoplankton blooms below snow-covered sea ice. Sci Rep 7:40850

Belt ST (2018) Source-specific biomarkers as proxies for Arctic and Antarctic sea ice. Org Geochem 125:277–298

Belt ST, Müller J (2013) The Arctic sea ice biomarker IP_{25}: a review of current understanding, recommendations for future research and applications in palaeo sea ice reconstructions. Quat Sci Rev 79:9–25

Belt ST, Massé G, Rowland SJ, Poulin M, Michel C, LeBlanc B (2007) A novel chemical fossil of palaeo sea ice: IP_{25}. Org Geochem 38:16–27

Belt ST, Brown TA, Rodriguez AN, Sanz PC, Tonkin A, Ingle R (2012) A reproducible method for the extraction, identification and quantification of the Arctic sea ice proxy IP_{25} from marine sediments. Anal Methods 4:705–713

Bluhm BA, Iken K, Mincks Hardy S, Sirenko BI, Holladay BA (2009) Community structure of epibenthic megafauna in the Chukchi Sea. Aquat Biol 7:269–293

Brown TA, Belt ST (2012) Closely linked sea ice–pelagic coupling in the Amundsen Gulf revealed by the sea ice diatom biomarker IP_{25}. J Plankton Res 34:647–654

Brown TA, Belt ST (2017) Biomarker-based H-Print quantifies the composition of mixed sympagic and pelagic algae consumed by Artemia sp. J Exp Mar Biol Ecol 488:32–37

Brown TA, Belt ST, Ferguson SH, Yurkowski DJ, Davison NJ, Barnett JEF, Jepson PD (2013) Identification of the sea ice diatom biomarker IP_{25} and related lipids in marine mammals: a potential method for investigating regional variations in dietary sources within higher trophic level marine systems. J Exp Mar Biol Ecol 441:99–104

Brown T, Alexander C, Yurkowski D, Ferguson S, Belt S (2014a) Identifying variable sea ice carbon contributions to the Arctic ecosystem: a case study using highly branched isoprenoid lipid biomarkers in Cumberland Sound ringed seals. Limnol Oceanogr 59:1581–1589

Brown TA, Belt ST, Tatarek A, Mundy CJ (2014b) Source identification of the Arctic sea ice proxy IP_{25}. Nat Commun 5:4197

Brown TA, Yurkowski DJ, Ferguson SH, Alexander C, Belt ST (2014c) H-Print: a new chemical fingerprinting approach for distinguishing primary production sources in Arctic ecosystems. Environ Chem Lett 12:387–392

Brown TA, Chrystal E, Ferguson SH, Yurkowski DJ and others (2017) Coupled changes between the H-Print biomarker and $\delta^{15}N$ indicates a variable sea ice carbon contribution to the diet of Cumberland Sound beluga whales. Limnol Oceanogr 62:1606–1619

Brown TA, Galicia MP, Thiemann GW, Belt ST, Yurkowski DJ, Dyck MG (2018) High contributions of sea ice derived carbon in polar bear (*Ursus maritimus*) tissue. PLOS ONE 13:e0191631

Budge SM, Wooller MJ, Springer AM, Iverson SJ, McRoy CP, Divoky GJ (2008) Tracing carbon flow in an arctic marine food web using fatty acid-stable isotope analysis. Oecologia 157:117–129

Cooper LW, Grebmeier JM (2018) Deposition patterns on the Chukchi shelf using radionuclide inventories in relation to surface sediment characteristics. Deep Sea Res II 152:48–66

Cooper LW, Grebmeier JM, Larsen IL, Dolvin SS, Reed AJ (1998) Inventories and distribution of radiocaesium in Arctic marine sediments: influence of biological and physical processes. Chem Ecol 15:27–46

Denisenko SG, Grebmeier JM, Cooper LW, Denisenko SG, Skvortsov VV (2015) Assessing bioresources and standing stock of zoobenthos (key species, high taxa, trophic groups) in the Chukchi Sea. Oceanography 28: 146–157

Dezutter T, Lalande C, Dufresne C, Darnis G, Fortier L (2019) Mismatch between microalgae and herbivorous copepods due to the record sea ice minimum extent of 2012 and the late sea ice break-up of 2013 in the Beaufort Sea. Prog Oceanogr 173:66–77

Divine LM, Bluhm BA, Mueter FJ, Iken K (2017) Diet analysis of Alaska Arctic snow crabs (*Chionoecetes opilio*) using stomach contents and $\delta^{13}C$ and $\delta^{15}N$ stable isotopes. Deep Sea Res II 135:124–136

Duffy-Anderson JT, Stabeno P, Andrews AG III, Cieciel K and others (2019) Responses of the northern Bering Sea and southeastern Bering Sea pelagic ecosystems following record-breaking low winter sea ice. Geophys Res Lett 46:9833–9842

Dunton KH, Grebmeier JM, Trefry JH (2014) The benthic ecosystem of the northeastern Chukchi Sea: an overview of its unique biogeochemical and biological characteristics. Deep Sea Res II 102:1–8

Encyclopedia of Life (2020) Global access to knowledge about life on Earth. https://eol.org (accessed 28 July 2020)

Falk-Petersen S, Sargent J, Henderson J, Hegseth E, Hop H, Okolodkov Y (1998) Lipids and fatty acids in ice algae and phytoplankton from the Marginal Ice Zone in the Barents Sea. Polar Biol 20:41–47

Feder HM, Naidu AS, Jewett SC, Hameedi JM, Johnson WR, Whitledge TE (1994) The northeastern Chukchi Sea: benthos–environmental interactions. Mar Ecol Prog Ser 111:171–190

Frey KE, Moore G, Cooper LW, Grebmeier JM (2015) Divergent patterns of recent sea ice cover across the Bering, Chukchi, and Beaufort seas of the Pacific Arctic Region. Prog Oceanogr 136:32–49

Frey KE, Comiso JC, Cooper LW, Grebmeier JM, Stock LV (2018) Arctic ocean primary productivity: the response of marine algae to climate warming and sea ice decline. Arctic Report Card 2018. https://arctic.noaa.gov/Report-Card/Report-Card-2018/ArtMID/7878/ArticleID/778/Arctic-Ocean-Primary-Productivity-The-Response-of-Marine-Algae-to-Climate-Warming-and-Sea-Ice-Decline

Gibbs P (1977) On the status of *Golfingia intermedia* (Sipuncula). J Mar Biol Assoc UK 57:109–112

Goethel CL, Grebmeier JM, Cooper LW (2019) Changes in abundance and biomass of the bivalve *Macoma calcarea* in the northern Bering Sea and the southeastern Chukchi Sea from 1998 to 2014, tracked through dynamic factor analysis models. Deep Sea Res II 162:127–136

Gradinger R (2009) Sea-ice algae: major contributors to primary production and algal biomass in the Chukchi and Beaufort Seas during May/June 2002. Deep Sea Res II 56:1201–1212

Grebmeier JM, Cooper LW (1995) Influence of the St. Lawrence Island polynya upon the Bering Sea benthos. J Geophys Res Oceans 100:4439–4460

Grebmeier JM, Cooper LW (2019a) Benthic macroinfaunal samples collected from the Canadian Coast Guard Ship (CCGS) Sir Wilfrid Laurier. Northern Bering Sea to Chukchi Sea, 2015. Arctic Data Center. https://arcticdata.io/catalog/view/doi:10.18739/A28W3827B

Grebmeier JM, Cooper LW (2019b) Surface sediment samples collected from the CCGS Sir Wilfrid Laurier 2018, Northern Bering Sea to Chukchi Sea. Arctic Data Center. https://arcticdata.io/catalog/view/doi:10.18739/A2C824F2J

Grebmeier JM, Cooper LW (2019c) Surface sediment samples collected from the United States Coast Guard Cutter Healy (HLY1801), Northern Bering Sea to Chukchi Sea. Arctic Data Center. https://arcticdata.io/catalog/view/doi:10.18739/A2H12V769

Grebmeier JM, Cooper LW, Feder HM, Sirenko BI (2006a) Ecosystem dynamics of the Pacific-influenced Northern Bering and Chukchi Seas in the Amerasian Arctic. Prog Oceanogr 71:331–361

Grebmeier JM, Overland JE, Moore SE, Farley EV and others (2006b) A major ecosystem shift in the northern Bering Sea. Science 311:1461–1464

Grebmeier JM, Moore SE, Overland JE, Frey KE, Gradinger R (2010) Biological response to recent Pacific Arctic sea ice retreats. EOS Trans Am Geophys Union 91:161–162

Grebmeier JM, Bluhm BA, Cooper LW, Danielson SL and others (2015) Ecosystem characteristics and processes facilitating persistent macrobenthic biomass hotspots and associated benthivory in the Pacific Arctic. Prog Oceanogr 136:92–114

Grebmeier JM, Frey KE, Cooper LW, Kędra M (2018) Trends in benthic macrofaunal populations, seasonal sea ice persistence, and bottom water temperatures in the Bering Strait region. Oceanography 31:136–151

Grubbs FE (1950) Sample criteria for testing outlying observations. Ann Math Stat 21:27–58

Hill V, Ardyna M, Lee SH, Varela DE (2018) Decadal trends in phytoplankton production in the Pacific Arctic Region from 1950 to 2012. Deep Sea Res II 152:82–94

Iken K, Bluhm B, Dunton K (2010) Benthic food-web structure under differing water mass properties in the southern Chukchi Sea. Deep Sea Res II 57:71–85

Jansen JM, Pronker AE, Kube S, Sokolowski A and others (2007) Geographic and seasonal patterns and limits on the adaptive response to temperature of European *Mytilus* spp. and *Macoma balthica* populations. Oecologia 154:23–34

Jay CV, Grebmeier JM, Fischbach AS, McDonald TL, Cooper LW, Hornsby F (2014) Pacific walrus (*Odobenus rosmarus divergens*) resource selection in the Northern Bering Sea. PLOS ONE 9:e93035

Kędra M, Moritz C, Choy ES, David C and others (2015) Status and trends in the structure of Arctic benthic food webs. Polar Res 34:23775

Kędra M, Grebmeier JM, Cooper LW (2018) Sipunculan fauna in the Pacific Arctic region: a significant component of benthic infaunal communities. Polar Biol 41:163–174

Kędra M, Cooper LW, Zhang M, Biasatti D, Grebmeier JM (2019) Benthic trophic sensitivity to on-going changes in Pacific Arctic seasonal sea ice cover—insights from the nitrogen isotopic composition of amino acids. Deep Sea Res II 162:137–151

Koch CW, Cooper LW, Lalande C, Brown TA, Frey KE, Grebmeier JM (2020) Seasonal and latitudinal variations in sea ice algae deposition in the Northern Bering and Chukchi Seas determined by algal biomarkers. PLOS ONE 15:e0231178

Kohlbach D, Graeve MA, Lange B, David C, Peeken I, Flores H (2016) The importance of ice algae-produced carbon in the central Arctic Ocean ecosystem: food web relationships revealed by lipid and stable isotope analyses. Limnol Oceanogr 61:2027–2044

Kohlbach D, Graeve M, Lange BA, David C and others (2018) Dependency of Antarctic zooplankton species on ice algae-produced carbon suggests a sea ice-driven pelagic ecosystem during winter. Glob Change Biol 24: 4667–4681

Kohlbach D, Ferguson SH, Brown TA, Michel C (2019) Landfast sea ice-benthic coupling during spring and potential impacts of system changes on food web dynamics in Eclipse Sound, Canadian Arctic. Mar Ecol Prog Ser 627:33–48

Kremer A, Stein R, Fahl K, Ji Z and others (2018) Changes in sea ice cover and ice sheet extent at the Yermak Plateau during the last 160 ka—reconstructions from biomarker records. Quat Sci Rev 182:93–108

Lalande C, Grebmeier JM, Hopcroft RR, Danielson SL (2020) Annual cycle of export fluxes of biogenic matter near Hanna Shoal in the northeast Chukchi Sea. Deep Sea Res II 177:104730

Legendre L, Ackley SF, Dieckmann GS, Gulliksen B and others (1992) Ecology of sea ice biota. 2. Global significance. Polar Biol 12:429–444

Lepore K, Moran S, Smith J (2009) ^{210}Pb as a tracer of shelf–basin transport and sediment focusing in the Chukchi Sea. Deep Sea Res II 56:1305–1315

Leu E, Søreide JE, Hessen DO, Falk-Petersen S, Berge J (2011) Consequences of changing sea-ice cover for primary and secondary producers in the European Arctic shelf seas: timing, quantity, and quality. Prog Oceanogr 90:18–32

Leu E, Mundy CJ, Assmy P, Campbell K and others (2015) Arctic spring awakening – steering principles behind the phenology of vernal ice algal blooms. Prog Oceanogr 139: 151–170

Lewis KM, van Dijken GL, Arrigo KR (2020) Changes in phytoplankton concentration now drive increased Arctic Ocean primary production. Science 369:198–202

Li WK, McLaughlin FA, Lovejoy C, Carmack EC (2009) Smallest algae thrive as the Arctic Ocean freshens. Science 326:539

Limoges A, Massé G, Weckström K, Poulin M and others (2018) Spring succession and vertical export of diatoms and IP_{25} in a seasonally ice-covered high Arctic fjord. Front Earth Sci 6:226

Macdonald TA, Burd B, Macdonald V, Van Roodselaar A (2010) Taxonomic and feeding guild classification for the marine benthic macroinvertebrates of the Strait of Georgia, British Columbia. Can Tech Rep Fish Aquat Sci 2874. Fisheries and Oceans Canada, Sidney, BC

Mäkelä A, Witte U, Archambault P (2017) Ice algae versus phytoplankton: resource utilization by Arctic deep sea macroinfauna revealed through isotope labelling experiments. Mar Ecol Prog Ser 572:1–18

McMahon KW, Ambrose WG Jr, Johnson BJ, Sun MY, Lopez GR, Clough LM, Carroll ML (2006) Benthic community response to ice algae and phytoplankton in Ny Ålesund, Svalbard. Mar Ecol Prog Ser 310:1–14

McTigue ND, Dunton KH (2014) Trophodynamics and organic matter assimilation pathways in the northeast Chukchi Sea, Alaska. Deep Sea Res II 102:84–96

Mincks SL, Smith CR, DeMaster DJ (2005) Persistence of labile organic matter and microbial biomass in Antarctic shelf sediments: evidence of a sediment 'food bank'. Mar Ecol Prog Ser 300:3–19

Mohan SD, Connelly TL, Harris CM, Dunton KH, McClelland JW (2016) Seasonal trophic linkages in Arctic marine invertebrates assessed via fatty acids and compound-specific stable isotopes. Ecosphere 7:e01429

Moore SE, Grebmeier JM (2018) The Distributed Biological Observatory: linking physics to biology in the Pacific Arctic region. Arctic 71(Suppl 1):1–7

Moore SE, Huntington HP (2008) Arctic marine mammals and climate change: impacts and resilience. Ecol Appl 18:S157–S165

Moore SE, Stabeno PJ (2015) Synthesis of Arctic Research (SOAR) in marine ecosystems of the Pacific Arctic. Prog Oceanogr 136:1–11

Moore SE, Stabeno PJ, Grebmeier JM, Okkonen SR (2018) The Arctic Marine Pulses Model: linking annual oceano-

graphic processes to contiguous ecological domains in the Pacific Arctic. Deep Sea Res II 152:8–21
Müller J, Stein R (2014) High-resolution record of late glacial and deglacial sea ice changes in Fram Strait corroborates ice–ocean interactions during abrupt climate shifts. Earth Planet Sci Lett 403:446–455
North CA, Lovvorn JR, Kolts JM, Brooks ML, Cooper LW, Grebmeier JM (2014) Deposit-feeder diets in the Bering Sea: potential effects of climatic loss of sea ice-related microalgal blooms. Ecol Appl 24:1525–1542
Overland JE, Stabeno PJ (2004) Is the climate of the Bering Sea warming and affecting the ecosystem? EOS Trans Am Geophys Union 85:309–312
Pickart RS, Weingartner TJ, Pratt LJ, Zimmermann S, Torres DJ (2005) Flow of winter-transformed Pacific water into the Western Arctic. Deep Sea Res II 52:3175–3198
Pickart RS, Nobre C, Lin P, Arrigo KR and others (2019) Seasonal to mesoscale variability of water masses and atmospheric conditions in Barrow Canyon, Chukchi Sea. Deep Sea Res II 162:32–49
Pirtle-Levy R, Grebmeier JM, Cooper LW, Larsen IL (2009) Chlorophyll *a* in Arctic sediments implies long persistence of algal pigments. Deep Sea Res II 56:1326–1338
Pisareva MN, Pickart RS, Iken K, Ershova EA and others (2015) The relationship between patterns of benthic fauna and zooplankton in the Chukchi Sea and physical forcing. Oceanography 28:68–83
R Core Team (2017) R: a language and environment for statistical computing. R Foundation for Statistical Computing, Vienna
Riedel A, Michel C, Gosselin M (2006) Seasonal study of sea-ice exopolymeric substances on the Mackenzie shelf: implications for transport of sea-ice bacteria and algae. Aquat Microb Ecol 45:195–206
Rontani JF, Smik L, Belt ST, Vaultier F, Armbrecht L, Leventer A, Armand LK (2019) Abiotic degradation of highly branched isoprenoid alkenes and other lipids in the water column off East Antarctica. Mar Chem 210:34–47
Schollmeier T, Oliveira A, Wooller M, Iken K (2018) Tracing sea ice algae into various benthic feeding types on the Chukchi Sea shelf. Polar Biol 41:207–224
Selz V, Laney S, Arnsten AE, Lewis KM and others (2018) Ice algal communities in the Chukchi and Beaufort Seas in spring and early summer: composition, distribution, and coupling with phytoplankton assemblages. Limnol Oceanogr 63:1109–1133
Serreze MC, Meier WN (2019) The Arctic's sea ice cover: trends, variability, predictability, and comparisons to the Antarctic. Ann N Y Acad Sci 1436:36–53
Sheffield G, Grebmeier JM (2009) Pacific walrus (*Odobenus rosmarus divergens*): differential prey digestion and diet. Mar Mamm Sci 25:761–777
Søreide JE, Leu EV, Berge J, Graeve M, Falk-Petersen S (2010) Timing of blooms, algal food quality and *Calanus glacialis* reproduction and growth in a changing Arctic. Glob Change Biol 16:3154–3163
Stabeno PJ, Bell SW (2019) Extreme conditions in the Bering Sea (2017–2018): record-breaking low sea-ice extent. Geophys Res Lett 46:8952–8959
Stein R, Fahl K, Schreck M, Knorr G and others (2016) Evidence for ice-free summers in the late Miocene central Arctic Ocean. Nat Commun 7:11148
Stein R, Fahl K, Gierz P, Niessen F, Lohmann G (2017) Arctic Ocean sea ice cover during the penultimate glacial and the last interglacial. Nat Commun 8:373
Sun MY, Clough LM, Carroll ML, Dai J, Ambrose WG Jr, Lopez GR (2009) Different responses of two common Arctic macrobenthic species (*Macoma balthica* and *Monoporeia affinis*) to phytoplankton and ice algae: Will climate change impacts be species specific? J Exp Mar Biol Ecol 376:110–121
Szymanski A, Gradinger R (2016) The diversity, abundance and fate of ice algae and phytoplankton in the Bering Sea. Polar Biol 39:309–325
Thoman RL, Bhatt US, Bieniek PA, Brettschneider BR and others (2020) The record low Bering Sea ice extent in 2018: context, impacts, and an assessment of the role of anthropogenic climate change. Bull Am Meteorol Soc 101:S53–S58
Thyrring J, Rysgaard S, Blicher ME, Sejr MK (2015) Metabolic cold adaptation and aerobic performance of blue mussels (*Mytilus edulis*) along a temperature gradient into the High Arctic region. Mar Biol 162:235–243
Tibshirani R, Walther G, Hastie T (2001) Estimating the number of clusters in a data set via the gap statistic. J R Stat Soc Ser B Stat Methodol 63:411–423
Tremblay JE, Michel C, Hobson KA, Gosselin M, Price NM (2006) Bloom dynamics in early opening waters of the Arctic Ocean. Limnol Oceanogr 51:900–912
Volkman JK, Barrett SM, Dunstan GA (1994) C_{25} and C_{30} highly branched isoprenoid alkenes in laboratory cultures of two marine diatoms. Org Geochem 21:407–414
Waga H, Hirawake T, Grebmeier JM (2020) Recent change in benthic macrofaunal community composition in relation to physical forcing in the Pacific Arctic. Polar Biol 43:285–294
Wang SW, Budge SM, Gradinger RR, Iken K, Wooller MJ (2014) Fatty acid and stable isotope characteristics of sea ice and pelagic particulate organic matter in the Bering Sea: tools for estimating sea ice algal contribution to Arctic food web production. Oecologia 174:699–712
Weingartner T, Fang YC, Winsor P, Dobbins E and others (2017) The summer hydrographic structure of the Hanna Shoal region on the northeastern Chukchi Sea shelf: 2011–2013. Deep Sea Res II 144:6–20

Editorial responsibility: Antonio Bode, A Coruña, Spain

Submitted: June 4, 2020; Accepted: August 19, 2020
Proofs received from author(s): September 27, 2020